Re-collectable and recyclable epichlorohydrin-crosslinked humic acid with spinel cobalt ferrite core for simple magnetic removal of cationic triarylmethane dyes in polluted water

by Mochamad Zakki Fahmi

Submission date: 01-Sep-2021 08:54PM (UTC+0800)
Submission ID: 1639430973
File name: e_and_recyclable_epichlorohydrin-crosslinked_humic_acid_with.pdf (3.61M)
Word count: 12194
Character count: 60948

Journal of Environmental Chemical Engineering 8 (2020) 104004

Contents lists available at ScienceDirect

Journal of Environmental Chemical Engineering

journal homepage: www.elsevier.com/locate/jece

Re-collectable and recyclable epichlorohydrin-crosslinked humic acid with spinel cobalt ferrite core for simple magnetic removal of cationic triarylmethane dyes in polluted water

Satya Candra Wibawa Sakti[a,b,*], Rahma Nuzulul Laily[a], Siti Aliyah[a], Nindayu Indrasari[a], Mochamad Zakki Fahmi[a,b], Hwei Voon Lee[c], Yasuhiro Akemoto[d,e], Shunitz Tanaka[d]

[a] Department of Chemistry, Faculty of Science and Technology, Universitas Airlangga, Campus C, Mulyorejo, Surabaya 60115, Indonesia
[b] Supramodification Nano-Micro Engineering Research Group, Universitas Airlangga, Campus C, Mulyorejo, Surabaya 60115, Indonesia
[c] Nanotechnology and Catalysis Research Centre, University of Malaya, Kuala Lumpur 50603, Malaysia
[d] Laboratory of Environmental Analysis and Remediation, Graduate School of Environmental Science, Hokkaido University, Kita 10, Nishi 5, Kita ku, Sapporo 060-0810, Japan
[e] Research Institute of Energy, Environment and Geology, Industrial Technology and Environment Research Department, Hokkaido Research Organization, Kita 19 Nishi 11, Kita ku, Sapporo 060-0819 Japan

ARTICLE INFO

Editor: Despo Kassinos

Keywords:
Spinel cobalt ferrite
Crosslinked humic acid
Adsorption
Basic fuchsin
Methyl violet 2B
Malachite green

ABSTRACT

Spinel cobalt ferrite ($CoFe_2O_4$) was successfully functionalized with humic acid ($CoFe_2O_4$-HA) via hydrothermal method. In order to prevent detachment, the humic acid layer on the $CoFe_2O_4$-HA surface was crosslinked with epichlorohydrin to obtain $CoFe_2O_4$-HA-ECH. Synthesized adsorbents were then tested for their ability to remove of basic fuchsin (BF), methyl violet 2B (MV), and malachite green (MG) from aqueous solutions. Particle size analysis, vibrating sample magnetometry, scanning electron microscopy, X-ray diffractometry, Fourier transform infrared spectrophotometry, thermogravimetric analysis, and ζ-potential analysis were conducted to characterize the as-synthesized adsorbents. The effects of adsorption parameters including pH, contact time, initial dye concentration, temperature, and ionic strength were explored. The kinetics data fitted well with a pseudo-second order model with Coefficient of Determination (R^2) ≥ 0.998, Chi-squared (χ^2) ≤ 0.171, and Average Relative Error (ARE) ≤ 3.443, suggesting that adsorption is the rate-limiting step. The Langmuir isotherm model provided R^2 ≥ 0.999, χ^2 ≤ 0.025, and ARE ≤ 0.891, indicating that adsorption occurs on a single layer on a homogenous surface. The maximum adsorption capacities of $CoFe_2O_4$-HA-ECH were 96.494, 62.627, and 48.74 μmol $\cdot g^{-1}$ for BF, MV, and MG, respectively, which were 10 times higher than those of $CoFe_2O_4$. Thermodynamic studies suggested that the adsorption processes are spontaneous-endothermic. Furthermore, $CoFe_2O_4$-HA-ECH can be re-collected and recycled for up to 10 cycles.

1. Introduction

Due to increasing industrialization, generated wastewaters that contain numerous types of noxious pollutants such as dyes, heavy metal ions, organic contaminants, fertilizer, pesticides, and pharmaceutical wastes are continuously being discharged into aquatic environments. Dyes containing wastewater generated from five major industries, i.e., textiles, dyeing, pulp and paper, tannery and paints, and dye manufacturing, have attracted the attention of researchers. More than 100,000 dyes are available commercially and up to 7×10^5 tonnes per year are manufactured [1]. Regrettably, about 15 % of produced dyes end up as pollutants in various aquatic environments [2]. Most of the artificial dyes are toxic [3], mutagenic [4], and carcinogenic [5] to both animals and humans.

Among various types of synthetic dyes, triarylmethane dyes are the most broadly used in the dyeing and textile industries because of their brilliant color and low cost [6]. The main structure of triarylmethane dyes is derived from the presence of monomethine with three terminal aryl groups as chromophores and functionalization using auxochromic groups such as hydroxyl, amino, or dimethyl amino [7]. A high tinctorial value and high dyeing efficiency are considered as beneficial properties of triarylmethane dyes. In addition to their extensive application to textiles, triarylmethane dyes are used for coloring drugs, foods, and cosmetics [8]. Basic fuchsin (BF), malachite green (MG), and

* Corresponding author at: Department of Chemistry, Faculty of Science and Technology, Universitas Airlangga, Campus C, Mulyorejo, Surabaya 60115, Indonesia.
E-mail address: satya.sakti@fst.unair.ac.id (S.C.W. Sakti).

https://doi.org/10.1016/j.jece.2020.104004
Received 6 March 2020; Received in revised form 21 April 2020; Accepted 28 April 2020
Available online 08 May 2020

methyl violet (MV) are the most applied triarylmethane dyes in the dye and pigment industry, which possess toxic, mutagenic, and carcinogenic features even at dilute concentrations. The presence of dye molecules in aquatic environments even at very low concentrations not only leads to unpleasant color and odor but also hinders sunlight penetration, disturbs photosynthetic activity, reduces dissolved O_2, and increases both biological and chemical oxygen demands [9,10]. Since the disadvantages of dyes were identified, numerous methods have been developed in recent years for clean-up of dye-polluted water and wastewater. These include membrane separation [11], catalysis-photocatalysis [12], coagulation-flocculation [13], electrochemical-Fenton oxidation [14], and use of biological techniques [15] and adsorption systems [16–20]. Adsorption methods have been broadly applied to eradicate dyes from various aquatic environments because they are highly efficient and cost-effective. Moreover, dyes are normally stable under various conditions because of their complex structures, which makes it difficult to treat them effectively by other methods. However, the adsorption methods are limited by the possibility of adsorbent loss during the adsorption process, which leads to secondary pollution, and the regeneration of adsorbents, which requires complex post-treatment methods. Some adsorbents also have slow kinetics or low adsorption capacity. Thus, it is essential to develop adsorbents that have rapid kinetics and high capacity, and are easy to re-collect and recycle.

Humic acid (HA) along with fluvic acid and humin are humic substances that are a major source of carbon in the biosphere and the main constituents of soil organic matter [21]. Moreover, HA is a ubiquitous macromolecule resulting from the decomposition of plants, animals, microorganisms, and other natural organic matter. The molecular weight, structure and chemical composition of HA strongly depend on its geographical origin, age, and environmental conditions [21]. However, HA has similar functional groups in its structure, dominated by phenolic and carboxylic acids. Other functional groups such as enolates, ethers, quinones, polysaccharides, and peptides can be found as well. HA has two types of sites in its macrostructure: (i) hydrophobic sites consisting of aromatic rings and aliphatic chains and (ii) hydrophilic sites consisting of hydroxyl and carboxylic groups. Both types of sites play a role in determining the properties of HA such as pH dependence, solubility, and interaction with other organic substances and heavy metal ions [22].

Due to its unique structure and properties, HA is widely used in environmental remediation. It has been reported that HA can be functionalized on an adsorbent [23], can act as a membrane [24] for removal of heavy metal ions [25], and can play a role in remediation of polluted water from dyes [26] and pesticides [27]. However, as it contains a fraction of humic substances, HA is insoluble in acidic water but becomes soluble under higher pH conditions, which limits its applications. The high solubility of HA due to the effects of pH and ionic strength causes HA-based adsorbents to become unstable and decreases their performance. This is a drawback for the application of HA for removal of pollutants in water.

Spinel cobalt ferrite ($CoFe_2O_4$) has received considerable attention due to its unique properties, including superparamagnetic properties, high saturation magnetization, notable mechanical strength, high surface area, and a modifiable surface [28]. $CoFe_2O_4$ is classified as a hard magnet that forms an inverse spinel structure with face centered cubic (fcc) symmetry. The metal ions occupy two positions, as an octahedral lattice and a tetrahedral lattice. All of the Co^{2+} ions are fixed in octahedral coordination while the Fe^{3+} ions are distributed uniformly in both octahedral and tetrahedral lattices [29]. Several routes have been developed to synthesize $CoFe_2O_4$, including coprecipitation [30], combustion [31], and hydrothermal [32], sono-chemical [33] and sol-gel methods [34]. Over the years, $CoFe_2O_4$ has been developed for environmental remediation and protection. It has been reported that $CoFe_2O_4$ can be employed as a catalyst and adsorbent for removal of some pollutants including toxic metal ions, dyes, and pesticides [35]. Easy recovery of $CoFe_2O_4$ at the end of a reaction by applying an external magnetic field is a superior feature to those of other non-magnetic adsorbents and catalysts. However, the $CoFe_2O_4$ structure collapses and loses most of its magnetic properties due to dissolution in acidic media resulting in free Co^{2+} and Fe^{3+} ions.

In the present study, HA-functionalized spinel cobalt ferrite ($CoFe_2O_4$-HA) was successfully prepared via a one-pot hydrothermal route. Epichlorohydrin was then used to crosslink with the HA and stabilize the complex from dissolution in basic media. The HA groups are connected to each other by covalent bonding with epichlorohydrin as a “bridge” and the obtained product is stable under a wide range of pH values. Furthermore, the structure of the synthesized crosslinked HA-functionalized $CoFe_2O_4$ ($CoFe_2O_4$-HA-ECH) was characterized by X-ray diffraction (XRD) analysis, scanning electron microscopy (SEM), Fourier transform infrared (FTIR) spectroscopy, thermal gravimetric analysis (TGA), and vibrating sample magnetometry (VSM). The as-prepared $CoFe_2O_4$-HA-ECH was successfully applied for a simple and rapid magnetic clean-up of basic fuchsin (BF), methyl violet (MF), and malachite green (MG) from aqueous solution. The clean-up performance of $CoFe_2O_4$-HA-ECH was evaluated by kinetic studies, and by isothermal and thermodynamic analysis. The clean-up mechanism of dyes by $CoFe_2O_4$-HA-ECH was studied with the help of zeta potential analysis. Due to the presence of magnetic $CoFe_2O_4$ particles, $CoFe_2O_4$-HA-ECH can be easily re-collected and regenerated magnetically up to 10 times without any noticeable loss of its adsorptive ability.

2. Experimental

2.1. Chemicals and materials

All reagents and chemicals used in the experiment were in analytical quality and applied as received without any extra pretreatment. For preparation of $CoFe_2O_4$ spinel preparation, cobalt(II) chloride hexahydrate ($CoCl_2.6H_2O$, 98–102 %) and iron(III) chloride hexahydrate ($FeCl_3.6H_2O$, 97 %) were supplied from Sigma-Aldrich, Germany. Humic acid was supplied by Wako, Japan. For magnetic-clean up experiments, three triarylmethane dyes namely: basic fuchsin (BF, $C_{19}H_{17}N_3.HCl$, > 85 %, Sigma-Aldrich, Germany), methyl violet 2B (MV, $C_{24}H_{27}N_3.HCl$, > 75 %, Sigma-Aldrich, Germany) and malachite green oxalate (MG, $C_{46}H_{50}N_4.2C_2HO_4.C_2H_2O_4$, 100 %, Wako, Japan) were used as target pollutants. Epichlorohydrin (C_3H_5ClO, 99 %) as crosslinker supplied by Sigma-Aldrich, Germany. Sodium hydroxide (NaOH, Merck, Germany) and hydrochloric acid (HCl, 37 %, Merck, Germany) were used as pH adjustor. Demineralized water was used in the preparation of all solutions.

2.2. Hydrothermal synthesis of HA-functionalized spinel cobalt ferrite ($CoFe_2O_4$-HA)

In brief, 0.4563 g of $CoCl_2.6H_2O$ (1.918 mmol) and 1.0368 g of $FeCl_3.6H_2O$ (3.834 mmol) were dissolved together in 20 ml of demineralized water and heated at 60 °C for 30 min under continuous stirring. The initial pH was set at 10 by adding 0.1 M NaOH solution. Five mL of 0.02 $g.mL^{-1}$ HA in 1 M NaOH solution was added dropwise into the mixture with continuous stirring for another 60 min and the mixture was subsequently poured into a Teflon-lined stainless autoclave. Basic conditions with a relatively high concentration of NaOH solution were selected for the synthesis of $CoFe_2O_4$ in order to prevent formation of impurities such as hematite and goethite [36]. The Teflon-lined stainless autoclave was kept at 180 °C for 24 h and allowed to cool down to room temperature. Higher temperature and longer hydrothermal time were avoided to prevent formation of carbon particles. The black solid product was collected from the autoclave using a neodymium magnet, rinsed with demineralized water repeatedly, and then freeze-dried. The product was labeled as $CoFe_2O_4$-HA. Bare $CoFe_2O_4$ was synthesized using similar steps and conditions without adding HA.

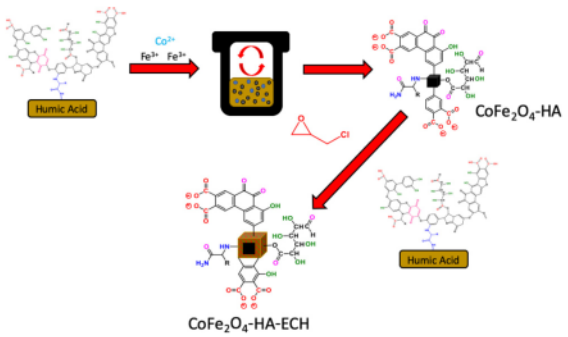

Scheme 1. Preparation of $CoFe_2O_4$ coated with epichlorohydrin-crosslinked humic acid.

2.3. Crosslinking of HA on the surface of spinel cobalt ferrite using epichlorohydrin

$CoFe_2O_4$-HA (1 g) obtained from a previous method was equilibrated in 25 ml ethanol and stirred at room temperature for 30 min. Twenty-five mL of 10 % epichlorohydrin in ethanol solution were added and the mixture was refluxed at 70 °C for 6 h under continuous stirring in order to allow the crosslinking reaction to be completed. The resultant black solid was re-collected magnetically, washed with ethanol several times, freeze dried, and labelled as $CoFe_2O_4$-HA-ECH. The as-synthesized $CoFe_2O_4$-HA-ECH obtained under this condition possesses a stable HA layer even in basic solution. The preparation of $CoFe_2O_4$ coated with epichlorohydrin-crosslinked HA is illustrated in Scheme 1.

2.4. Physicochemical measurements and characterizations

The synthesized $CoFe_2O_4$, $CoFe_2O_4$-HA and $CoFe_2O_4$-HA-ECH were characterized as follow. Crystal structure formation was determined using an X-ray diffractometer (PANalytical X'Pert Pro-MPD, Germany) with Cu Kα irradiation source (λ = 0.154 nm) at 30 kV and 15 mA. Analysis was conducted at room temperature over 2θ ranged from 5 to 80° at scanning rate 5°.min^{-1}. The Joint Committee on Powder Diffraction Standards (JCPDS) data library were used to identify the crystal structure of synthesized $CoFe_2O_4$, $CoFe_2O_4$-HA and $CoFe_2O_4$-HA-ECH. The morphology was explored by using a scanning electron microscope (JEOL, JSM-6360-LA, Japan). Infrared spectra of $CoFe_2O_4$, $CoFe_2O_4$-HA and $CoFe_2O_4$-HA-ECH were recorded on a Fourier transformed infrared spectrophotometer (IRTracer-100, Shimadzu, Japan) in the ranged from 4000 − 500 cm^{-1} using KBr disk method. Delsa™ Nano HC Zeta Potential (Backman Coulter Inc, USA) was used to determine surface zeta potential of $CoFe_2O_4$, $CoFe_2O_4$-HA and $CoFe_2O_4$-HA-ECH in the pH ranged from 2 to 12. For surface ζ-potential measurement, pH of solution was adjusted by using Delsa™ Nano AT Auto titrator (Backman Coulter Inc, USA). Average particle size of synthesized $CoFe_2O_4$, $CoFe_2O_4$-HA and $CoFe_2O_4$-HA-ECH were measured with a particle size analyzer (Microtrac MT3300EX, Nikkiso. Co.Ltd, Japan). The magnetic properties of synthesized $CoFe_2O_4$, $CoFe_2O_4$-HA and $CoFe_2O_4$-HA-ECH were examined using a vibrating sample magnetometer (Lake Shore 7400 Series). The examination was conducted at room temperature with maximum applied magnetic field of 8000 Oe. Thermal stability of $CoFe_2O_4$, $CoFe_2O_4$-HA and $CoFe_2O_4$-HA-ECH were investigated by using a thermogravimetric analyzer (TGA – 4000 Perkin Elmer, USA) from room temperature to 800 °C with a heating rate of 5 °C.min^{-1} under helium atmosphere.

2.5. Magnetic clean-up of BF, MV, and MG

The batch magnetic clean-up of triarylmethane dyes from solution were conducted by dispersing 0.01 g of $CoFe_2O_4$, $CoFe_2O_4$-HA and $CoFe_2O_4$-HA-ECH in series of 30 ml glass bottles containing 20 ml of 100 µmol.L^{-1} BF, MG or MV solution. Initial pH of BF, MG, and MV solution was adjusted by using 0.01 mol.L^{-1} HCl or NaOH solution. The mixtures were equilibrated in a mechanical shaker for 2 h at a constant speed of 300 rpm and after reached equilibrium stage, $CoFe_2O_4$, $CoFe_2O_4$-HA and $CoFe_2O_4$-HA-ECH were separated magnetically by using a neodymium magnet. Final concentration of BF, MG and MV in solution were measured by determining absorbance using a UV–vis Spectrofotometer at 540, 582 and 617 nm, respectively. The amount of removed BF, MG, and MV at equilibrium stage per g of $CoFe_2O_4$, $CoFe_2O_4$-HA and $CoFe_2O_4$-HA-ECH (q_e, µmol. g^{-1}) were determined based on Eq. (1) below:

$$q_e = \frac{(C_0 - C_{eq}) \cdot V}{m} \quad (1)$$

where C_0 and C_{eq} are the concentration of BF, MG, and MV in the solution at initial and equilibrium stage (µmol.L^{-1}), respectively; V is volume of the BF, MG, and MV solution (L) and m is the mass (g) of $CoFe_2O_4$, $CoFe_2O_4$-HA and $CoFe_2O_4$-HA-ECH.

A series of 30 ml glass bottles containing 20 ml of 100 µmol.L^{-1} BF, MG or MV solution were placed in a mechanical shaker and 0.01 g of $CoFe_2O_4$, $CoFe_2O_4$-HA or $CoFe_2O_4$-HA-ECH was added to each bottle. The mixtures were equilibrated at different time interval ranging from 0 to 120 min under constant agitation speed of 300 rpm. The kinetics parameters were determined from contact time dependent data. The experimental data were then simulated with the pseudo-first order (PFO), pseudo-second order (PSO) and Elovich kinetics models. Isotherm parameters were investigated by equilibrating $CoFe_2O_4$, $CoFe_2O_4$-HA and $CoFe_2O_4$-HA-ECH with BF, MG, and MV solution with initial concentration ranged from 10 to 800 µmol.L^{-1}. The Langmuir, Freundlich and Temkin isotherms models were employed to simulate the experimental data.

2.6. Error analysis

The most suitable kinetics and isotherms model was selected by fitting the experimental data with the non-linearized kinetics (pseudo-first order, pseudo-second order and Elovich models) or isotherm models (the Langmuir, Freundlich and Temkin models) based on Coefficient of Determination (R^2), Chi-squared (χ^2) and Average Relative Error (ARE) analyses as presented in Eqs. (2–4):

$$R^2 = \frac{\sum (q_{e,m} - \bar{q}_{e,e})^2}{\sum (q_{e,m} - \bar{q}_{e,e})^2 + (q_{e,m} - q_{e,e})^2} \quad (2)$$

$$\chi^2 = \sum \frac{(q_{e,e} - q_{e,m})^2}{q_{e,m}} \quad (3)$$

$$ARE = \frac{100}{n} \sum_{i=1}^{n} \left| \frac{q_{e,e} - q_{e,m}}{q_{e,e}} \right|_i \quad (4)$$

where $q_{e,e}$ and $\bar{q}_{e,e}$ are the equilibrium capacity and the average equilibrium capacity of $CoFe_2O_4$, $CoFe_2O_4$-HA and $CoFe_2O_4$-HA-ECH toward BF, MG, and MV obtained from experimental data (µmol. g^{-1}), respectively. The $q_{e,m}$ is the equilibrium capacity obtained from non-linearized model (µmol. g^{-1}). Kinetics and isotherm model which generated minimum error value are selected as the best models.

2.7. Recycle and regeneration for magnetic clean-up of BF, MV, and MG

Consecutive cycles of adsorption, desorption and re-adsorption were performed in order to evaluate the regeneration ability of $CoFe_2O_4$,

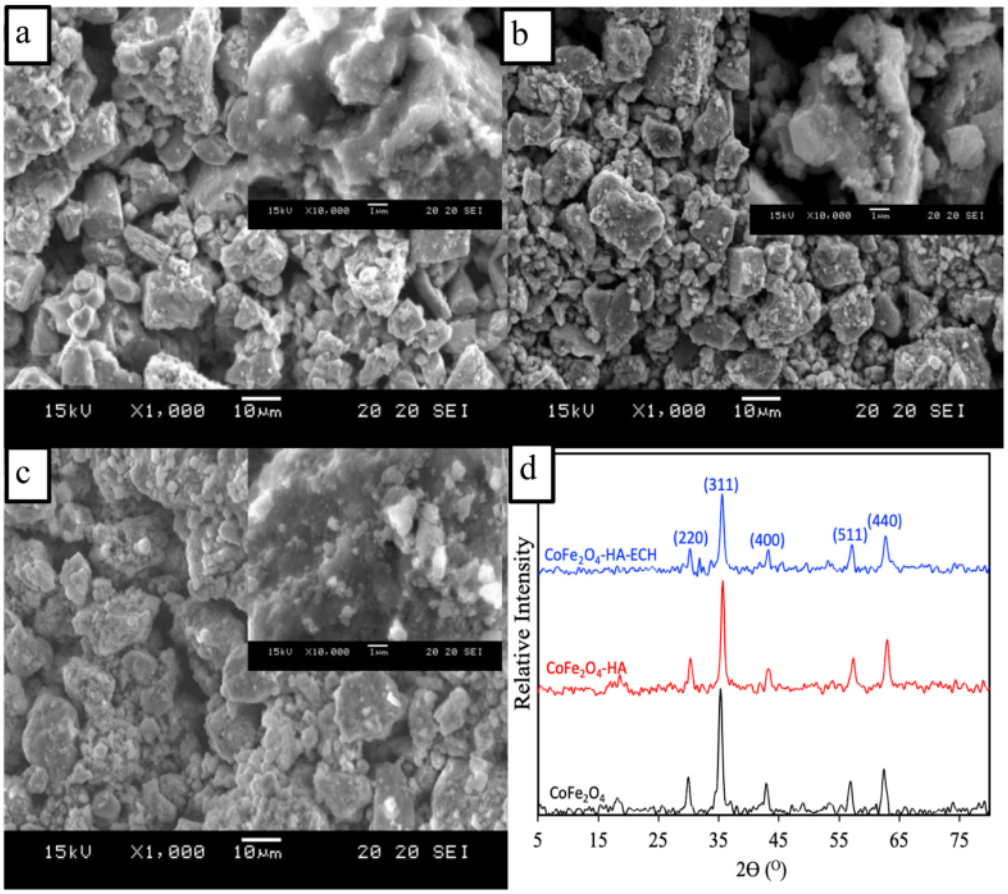

Fig. 1. SEM micrograph at 1000 magnification (inset: 10.000 magnification) of $CoFe_2O_4$ (a), $CoFe_2O_4$-HA (b), $CoFe_2O_4$-HA-ECH (c) and X-ray diffractogram of $CoFe_2O_4$, $CoFe_2O_4$-HA and $CoFe_2O_4$-HA-ECH (d).

$CoFe_2O_4$-HA and $CoFe_2O_4$-HA-ECH. $CoFe_2O_4$, $CoFe_2O_4$-HA and $CoFe_2O_4$-HA-ECH (0.01 g) were equilibrated with 20 ml of 100 μmol.L^{-1} BF, MG, and MV solution for 2 h at optimum pH obtained from previous adsorption experimental data. The $CoFe_2O_4$, $CoFe_2O_4$-HA and $CoFe_2O_4$-HA-ECH were then re-collected from the mixture and concentration of BF, MG, and MV were measured by using an UV–vis spectrophotometer. A 20 ml of 10 wt.% NaCl in 25 % acetic acid solution was then added to the bottles containing dye-adsorbed $CoFe_2O_4$, $CoFe_2O_4$-HA and $CoFe_2O_4$-HA-ECH to desorp the adsorbed dyes. The amount of desorbed BF, MG, and MV from $CoFe_2O_4$, $CoFe_2O_4$-HA and $CoFe_2O_4$-HA-ECH in the mixture were measured by using an UV–vis spectrophotometer.

3. Results and discussion

3.1. Physicochemical characteristics of $CoFe_2O_4$-HA-ECH

3.1.1. Morphology, structure, and particle size

SEM images of as-prepared $CoFe_2O_4$, $CoFe_2O_4$-HA and $CoFe_2O_4$-HA-ECH are presented in Fig. 1(a–c). The micrographs show that $CoFe_2O_4$ has a rough surface and irregular particle shape. The $CoFe_2O_4$ forms aggregates, because of the strong interaction among $CoFe_2O_4$ particles due to their magnetic nature [37]. A similar result was obtained by synthesis of $CoFe_2O_4$ via combustion, precipitation, and co-precipitation [38]. The rough surface and irregular shape of $CoFe_2O_4$ are not significantly altered after functionalization with HA and crosslinking with epichlorohydrin.

The as-synthesized $CoFe_2O_4$, $CoFe_2O_4$-HA, and $CoFe_2O_4$-HA-ECH were characterized using an X-ray diffractometer in order to investigate their structures; the XRD patterns are shown in Fig. 1d. The peaks observed at around 30.06°, 35.37°, 43.03°, 57.03°, and 62.56° indicate the presence of (220), (311), (400), (511), and (440) planes, respectively, which is consistent with the cubic phase of $CoFe_2O_4$ (JCPDS Card No. 22-1086). No other peaks of impurities such as Fe_2O_3 or CoO are observed, indicating high purity of $CoFe_2O_4$ [39]. The same peaks can also be observed in the XRD patterns of $CoFe_2O_4$-HA and $CoFe_2O_4$-HA-ECH with lower peak intensity, indicating decreased crystallinity after functionalization. However, all crystal structures of the synthesized $CoFe_2O_4$, $CoFe_2O_4$-HA, and $CoFe_2O_4$-HA were similar and found to be of the inverse spinel type with cubic symmetry. The spinel type structure is sustained even after modification with HA and crosslinking with epichlorohydrin. A similar phenomenon was observed on coating $CoFe_2O_4$ with other matrices such as SiO_2 [40] and chitosan [41].

3.1.2. FTIR analysis

Determination of functional groups on the surfaces of $CoFe_2O_4$, $CoFe_2O_4$-HA, and $CoFe_2O_4$-HA-ECH was conducted by FTIR analysis, and the results are presented in Fig. 2a. The FTIR spectra of all obtained samples were used to evaluate the alteration of the $CoFe_2O_4$ surface after modification with HA and crosslinking with epichlorohydrin. The

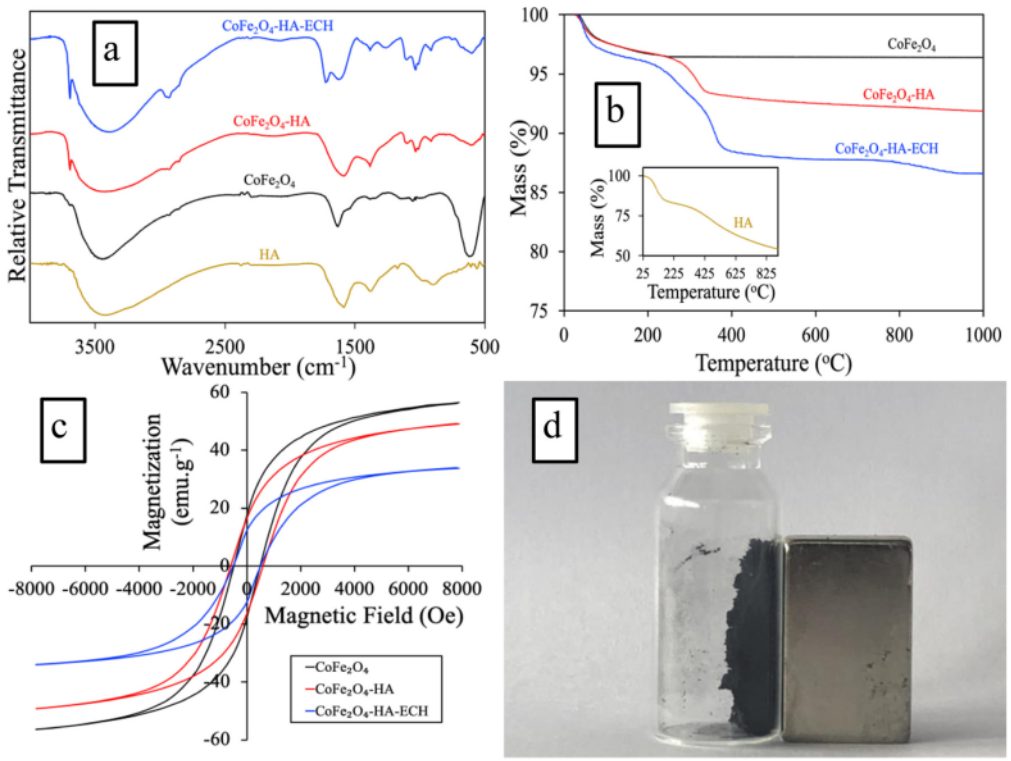

Fig. 2. FTIR spectra (a) thermogravimetric analysis curves (b) and magnetization curves (c) of $CoFe_2O_4$, $CoFe_2O_4$-HA, $CoFe_2O_4$-HA-ECH and images of $CoFe_2O_4$-HA-ECH attracted by magnet (d).

characteristics of $CoFe_2O_4$ were examined. The O—H stretching vibration of free adsorbed water is represented by two peaks, one at 3417 cm^{-1} and another at 1625 cm^{-1}. The metal oxide bond vibration observed at 594 cm^{-1} corresponds to the Fe-O or Co-O stretching vibration of spinel ferrite [41].

Non-magnetic bare HA is characterized by the presence of CH_2 scissoring at 1363 cm^{-1}. The O—H stretching vibration is observed at 3410 cm^{-1} [42]. The peaks at 1581 cm^{-1} and 1161 cm^{-1} are ascribed to N—H deformation and C—OH stretching vibration of aliphatic —OH, respectively. A new peak can clearly be observed around 1382 cm^{-1} after modification of $CoFe_2O_4$ with HA, which also can be found on coating of Fe_3O_4 with HA. This new peak ascribed to the CH_2 scissoring mode indicates the presence of HA on the surface of $CoFe_2O_4$-HA [43]. Further crosslinking by using epichlorohydrin is confirmed by peaks that appear at 1712 and 2922 cm^{-1}, which are associated with the C=O stretching vibration of the ester group and C–H stretching of the methylene group, respectively [44]. The appearance of some specific peaks of HA and epichlorohydrin indicates that modification of $CoFe_2O_4$ with HA and crosslinking with epichlorohydrin were successfully conducted.

3.1.3. Stability of $CoFe_2O_4$-HA-ECH at various temperatures

Thermogravimetric analysis was conducted in order to determine the weight loss of $CoFe_2O_4$, $CoFe_2O_4$-HA, and $CoFe_2O_4$-HA-ECH, where the amount of non-magnetic-organic layer coated on the surface of $CoFe_2O_4$ was measured. The TGA analyses were conducted in a He atmosphere in order to avoid oxidation of the organic layer by O_2 at high temperature. The results of TGA analysis are presented in Fig. 2b. At a temperature range of 30–200 °C, bare $CoFe_2O_4$ only lost about 3.26 % of its mass due to evaporation of physical water molecules on its surface. The mass of $CoFe_2O_4$ remained stable and no obvious mass loss was observed in the temperature range 200–1000 °C.

The thermal degradation of HA can be divided into 4 reaction stages. In stage 1 (30–200 °C), HA loses 16.42 % of its mass due to evaporation of adsorbed water and volatile molecules on the surface. Stage 2 (200–300 °C) is associated with decarboxylation of acidic groups, dehydration of aliphatic structures bearing hydroxyl groups, and thermal decomposition of polysaccharides. Thermal degradation due to pyrolysis of the aliphatic chain occurs in stage 3 (300–375 °C). Stage 4 (375–900 °C) is mainly due to decomposition of aliphatic acids, decarboxylation of acidic sites, and breakdown of aromatic rings. Bare HA loses 2.4 %, 2.83 %, and 39.5 % of mass in stages 2, 3, and 4, respectively. Both $CoFe_2O_4$-HA and $CoFe_2O_4$-HA-ECH lose the major fraction of mass at temperatures higher than 200 °C due to thermal degradation of HA and epichlorohydrin-crosslinked HA. At 1000 °C (final temperature), the mass losses of $CoFe_2O_4$-HA and $CoFe_2O_4$-HA-ECH were 7.97 % and 13.17 %, respectively.

3.1.4. Characterization of magnetic properties

The magnetization curves of the prepared $CoFe_2O_4$, $CoFe_2O_4$-HA, and $CoFe_2O_4$-HA-ECH measured at room temperature are presented in Fig. 2c. Several important magnetic parameters including saturation magnetization (Ms), coercivity (Hc), remanent magnetization (Mr), and value of squareness (Mr/Ms) are all listed in Table 1. A hysteresis loop can be found in all the magnetization curves, indicating that $CoFe_2O_4$, $CoFe_2O_4$-HA, and $CoFe_2O_4$-HA-ECH have ferromagnetic characteristics with high Mr and Hc values. From Fig. 2c and Table 1, it can be seen that $CoFe_2O_4$ shows the highest Ms value than $CoFe_2O_4$-HA and $CoFe_2O_4$-HA-ECH. However, the Ms value of $CoFe_2O_4$ is lower than the reported value for bulk inverse $CoFe_2O_4$ (80 $emu.g^{-1}$) [45]. Differences in particle shape, size, and homogeneity of the surface result from different synthesis methods and could lead to different Ms values.

Table 1
Magnetic-physical properties of $CoFe_2O_4$, $CoFe_2O_4$-HA and $CoFe_2O_4$-HA-ECH.

Magnetic Adsorbent	Non-magnetic Organic Modifier	Average Particle Size[a] (μm)	Ms[b] (emu. g^{-1})	Hc[b] (G)	Mr[b] (emu. g^{-1})	Mr/Ms
$CoFe_2O_4$	–	37.85	56.408	598.040	17.579	0.311
$CoFe_2O_4$-HA	Humic acid	58.86	49.233	509.380	16.420	0.333
$CoFe_2O_4$-HA-ECH	Epichlorohydrin-crosslinked humic acid	80.73	34.009	491.550	12.317	0.362

[a] measured by using a particle size analyser.
[b] measured by using a vibrating sample magnetometer.

The magnetization of the synthesized $CoFe_2O_4$-HA and $CoFe_2O_4$-HA-ECH is 12 % and 40 % lower than that of $CoFe_2O_4$. This suggests that the presence of the HA and HA-ECH layers reduce the magnetization of $CoFe_2O_4$. The HA and HA-ECH layers are diamagnetic and do not contribute to the magnetization properties of $CoFe_2O_4$. The coating of HA and HA-ECH layers on the $CoFe_2O_4$ surface facilitates mass gain and large particle sizes; however, this organic layer is able to reduce self-interaction of $CoFe_2O_4$ particles due to its magnetization properties. In additional, functionalized $CoFe_2O_4$ can be easily separated as bulk $CoFe_2O_4$ from water by the use of a magnet. This achievement implies that the magnetization of $CoFe_2O_4$, $CoFe_2O_4$-HA, and $CoFe_2O_4$-HA-ECH is sufficiently high for the application of magnetic clean-up in the treatment of dye-polluted water.

3.2. Magnetic clean-up of BF, MV, and MG

3.2.1. pH-dependent adsorption and magnetic removal mechanism

The initial pH of solution is well known as one of the critical factors that determine the dye removal performance of adsorbents. It determines the degree of ionization of adsorptive molecules and their interaction with the charged surface of the adsorbents [10]. The amounts of BF, MV, and MG adsorbed by $CoFe_2O_4$, $CoFe_2O_4$-HA, and $CoFe_2O_4$-HA-ECH as a function of pH are presented in Fig. 3(b–d). The amounts adsorbed by $CoFe_2O_4$-HA-ECH strongly increases as the pH increases from 3 to 7 and then slightly decreases as the pH increases to 11. Due to the presence of crosslinked HA, $CoFe_2O_4$-HA-ECH shows a higher performance than $CoFe_2O_4$-HA at all pH values, whereas bare $CoFe_2O_4$ hardly removes any of the dyes from solution. Also, pH 7 was found to be the optimum pH for magnetic removal of the dyes by all as-prepared magnetic adsorbents.

Zeta-potential measurement can be conducted to confirm the interaction mechanism between adsorbents and dyes in a solution [46]. As shown in Fig. 3a, ζ-potentials of $CoFe_2O_4$ ranged from 9.28 to -19.08 mV at pH 2–12, which shows that the surface of $CoFe_2O_4$ is positively charged in the acidic solution and negatively charged under the alkaline condition, while HA exhibits slightly different behavior. HA possesses a stable negative charge from pH 2–12, with ζ-potentials ranging from -17.45 to -58.56 mV. Both $CoFe_2O_4$-HA and $CoFe_2O_4$-HA-ECH are also negatively charged over the entire range of examined pH due to the presence of abundant carboxylic acid groups in the HA layer on the surface of the adsorbents [43]. Thus, the functional-group-richness of the HA layers results in the lowest ζ-potential of $CoFe_2O_4$-HA-ECH among the three adsorbents, which leads to the highest removal performance for the three dyes.

Intensive electrostatic interaction between negatively charged $CoFe_2O_4$-HA-ECH with positively charged BF, MV, and MG led to a high removal performance. Electrostatic interaction in acidic solution is unfavorable due to the presence of H^+ which competes with the dyes to interact with the $CoFe_2O_4$-HA-ECH surface. Furthermore, electrostatic repulsion occurs between bare $CoFe_2O_4$ and the dyes in acidic solution due to the presence of a positive charge. Similar phenomena were also reported by other researchers [47–49]. The presence of hydroxide ion (OH^-) results in competition with $CoFe_2O_4$-HA-ECH to interact with the dyes, leading to a slightly lower removal efficiency at higher pH. In addition to electrostatic interaction, other interactions such as π-π interactions and hydrogen bonding may also be responsible for the dye removal mechanism by the as-synthesized spinel ferrite-based adsorbents [35]. A proposed magnetic removal mechanism of the dyes is presented in Scheme 2.

3.2.2. Contact time dependent adsorption

The effect of contact time on removal of the dyes by the adsorbents was analyzed with an initial dye concentration of 100 μmol.L^{-1} using an adsorbent dosage of 2 g.L^{-1} at 25 °C and pH 7 (the optimum pH). The dye removal efficiency as a function of contact time is presented in Fig. 4. The amount of adsorbed dyes rapidly increases for the first 10 min due to a high availability of active adsorption sites on the surface of the adsorbent [46]. The amount of adsorbed dyes then moderately increases and reaches an equilibrium after 30 min. This phenomenon is attributed to a decrease in the availability of active adsorption sites on the surface of the adsorbent and thus reduced contact accessibility due to competition among the dye molecules [49]. High surface coverage and fewer active sites slows down the removal rate of the dyes by $CoFe_2O_4$-HA-ECH. Both $CoFe_2O_4$ and $CoFe_2O_4$-HA removed the dyes from solution, similar to the behavior of $CoFe_2O_4$-HA-ECH at all ranges of studied contact time.

3.2.3. Effect of dye initial concentration

A systematic assessment of the adsorption capacity of $CoFe_2O_4$-HA-ECH for BF, MV, and MG by varying the initial concentration of the dyes plays a vital role in determining its maximum capacity and provides essential information related to the removal mechanism. The initial dye concentration was varied at pH 7 with a dye-adsorbent contact time of 2 h, and the results are presented in Fig. 5(a–c). A contact time of two hours was selected to make sure the equilibrium stage was reached, even though experimental data indicated that 30 min was sufficient. As shown in Fig. 5(a–c), the adsorption efficiency is dependent on the initial dye concentrations. At low initial concentration, the q_e value increases rapidly then gradually approaches a constant value as the initial concentration increases further. Enhanced adsorption capacity of $CoFe_2O_4$-HA-ECH at a lower dye concentration occurs due to a high ratio of free-active adsorption sites to the number of dye molecules. At equilibrium, the BF, MV, and MG mass gradient between the solution and $CoFe_2O_4$-HA-ECH becomes steady, which explains the plateau area of the curves. As shown in Fig. 5, the amount of dye adsorbed by $CoFe_2O_4$-HA-ECH followed the order BF > MV > MG. This indicates that the affinity of $CoFe_2O_4$-HA-ECH for BF is significantly higher than that for MV and MG.

3.3. Kinetics study

From a kinetics point of view, the removal of dyes by the adsorbents is considered a complex mechanism which involves electrostatic interaction, hydrogen linkage, and π-π interactions. Exploring the adsorption kinetics is essential in order to obtain a better understanding of the removal mechanism. The rate controlling step of dye removal was evaluated by simulating the experimental data with various kinetic models such as pseudo-first order (PFO) [50], PSO [51] and Elovich [52] models. Mathematical formulas for non-linearized PSO (Eq. 5), PSO (Eq. 6) and Elovich (Eq. 7) models are expressed as follows:

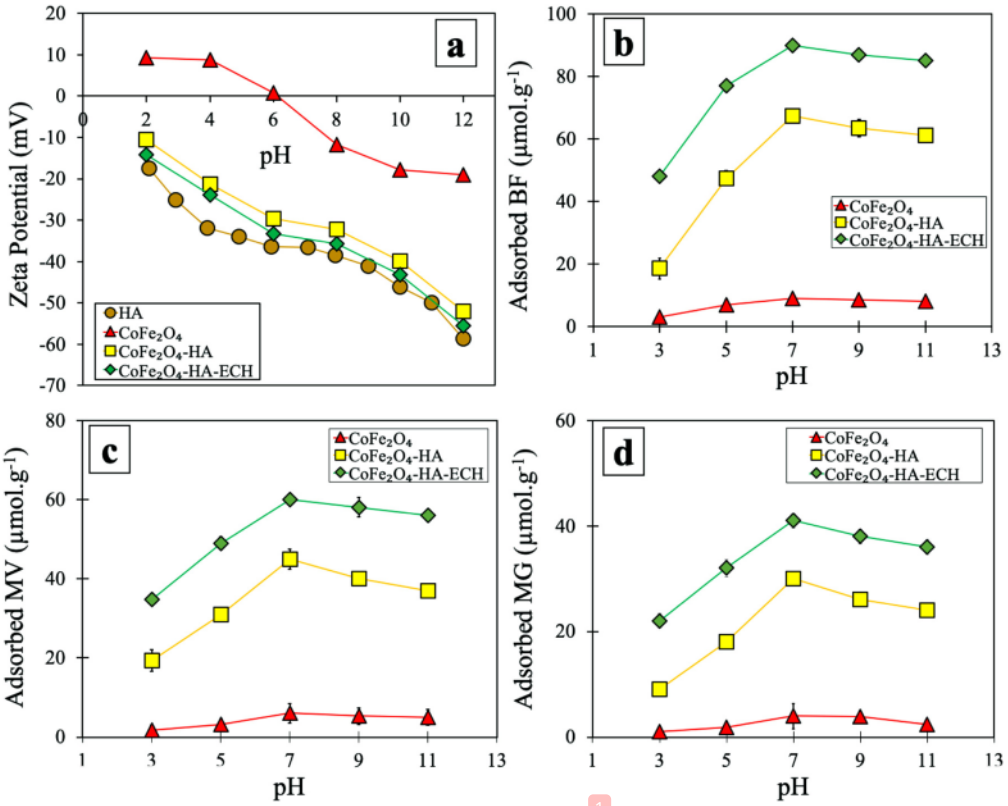

Fig. 3. ζ-potential value of HA, $CoFe_2O_4$, $CoFe_2O_4$-HA and $CoFe_2O_4$-HA-ECH in various pH (a), effect of solution initial pH on magnetic clean-up of BF (b), MV (c) and MG (d) by $CoFe_2O_4$, $CoFe_2O_4$-HA and $CoFe_2O_4$-HA-ECH (Experiment condition: C_0: 100 µmol.L^{-1}, t: 2 h, T: 25 °C, adsorbent dose: 2 g.L^{-1} and n: 3).

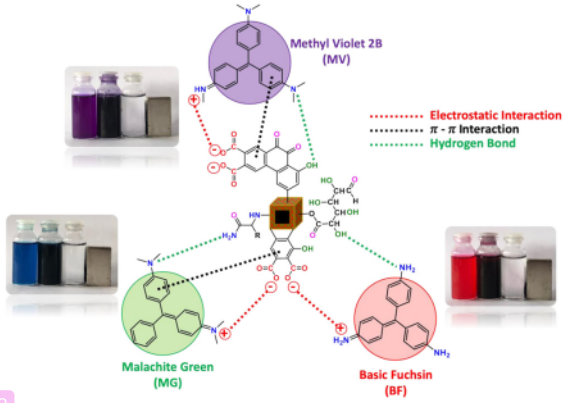

Scheme 2. Proposed magnetic removal mechanism of BF, MV, and MG by $CoFe_2O_4$-HA-ECH.

$$q_t = q_e(1 - exp(-K_{PFO}t)) \quad (5)$$

$$q_t = \frac{K_{PSO}.\ q_e^2.\ t}{1 + (q_e.\ K_{PSO}.\ t)} \quad (6)$$

$$q_t = \beta^{-1}Ln(\alpha\beta t) \quad (7)$$

where q_t and q_e are the amounts of adsorbed dyes (µmol·g^{-1}) at time t (min) and at equilibrium, K_{PFO} and K_{PSO} are the pseudo-first order (min^{-1}) and the pseudo-second order (g·µmol^{-1}·min^{-1}) rate constants, α is the initial adsorption rate (µmol.g^{-1}.min^{-1}), and β is the Elovich kinetics model parameter which is related to surface coverage (g·µmol^{-1}). The results of non-linear evaluation of the experimental data with the PFO, PSO, and Elovich models are shown in Fig. 4 and all calculated parameters are listed in Table 2. Based on the results of error analysis, fitting the experimental data with the PFO and the Elovich kinetics models generated low R^2 values and high χ^2 and ARE values, indicating that neither the PFO nor Elovich kinetics models are relevant for describing the adsorption mechanism. On the other hand, the calculated kinetics parameters show excellent agreement with the PSO kinetics model, attaining the highest R^2 and lowest χ^2 and ARE values in comparison with those from the PFO and Elovich models, implying that chemisorption is the rate-controlling step. Additionally, the q_e values obtained from the PSO kinetics model are in close agreement with the maximum adsorption capacity (q_{max}) obtained from isotherm studies (section 3.4). The formation of HA on the $CoFe_2O_4$-HA surface and crosslinked HA on the $CoFe_2O_4$-HA-ECH surface provides an abundance of active adsorption sites. Active adsorption sites are approachable by the dye molecules without any significant hindrance, dominated by electrostatic interaction, leading to rapid removal of the dyes from bulk solution.

3.4. Isotherm studies

Adsorption isotherm evaluations were systematically conducted not only to determine the maximum capacities of the adsorbents but also to figure out their interaction with the dyes at equilibrium. The experimental data for dye removal at equilibrium were fitted to the Freundlich (Eq. 8) [53], Langmuir (Eq. 9) [54], and Temkin (Eq. 10)

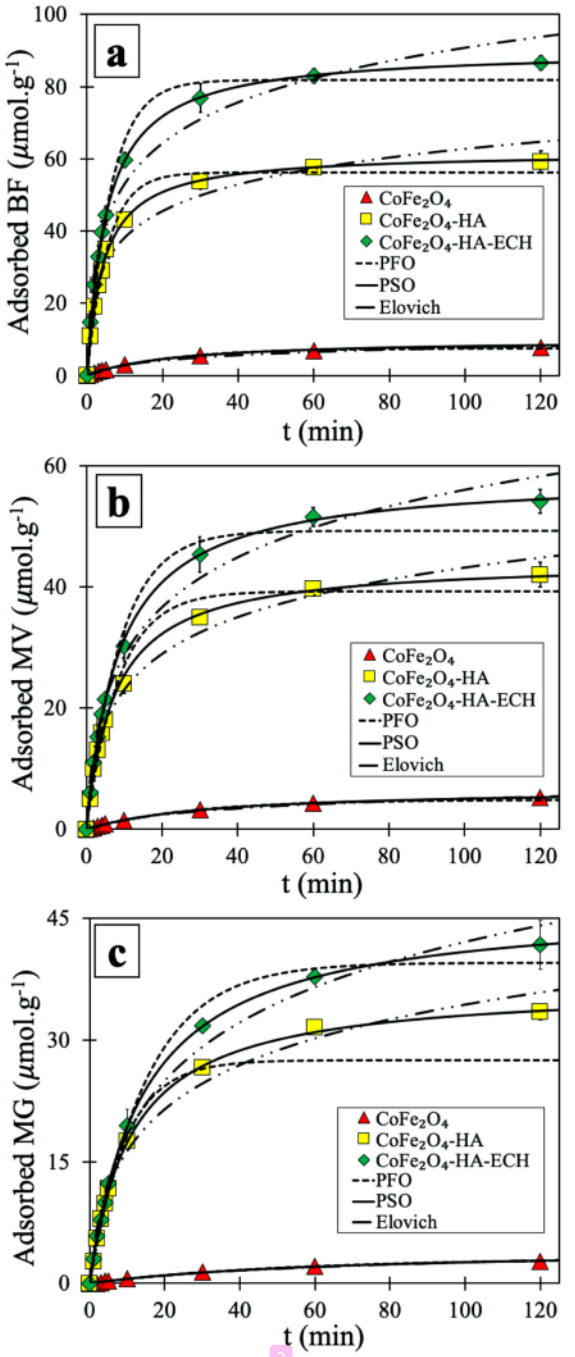

Fig. 4. Kinetics experimental data of magnetic removal of BF (a), MV (b) and MG (c) by $CoFe_2O_4$, $CoFe_2O_4$-HA and $CoFe_2O_4$-HA-ECH fitted with the non-linear pseudo-first order, pseudo-second order and Elovich models (Experiment condition: C_0: 100 μmol.L^{-1}, pH 7, t: 2 h, T: 25 °C, adsorbent dose: 2 g.L^{-1} and n: 3).

[55] isotherm models which can be expressed as follows:

$$q_e = K_F (C_e)^{\frac{1}{n}} \quad (8)$$

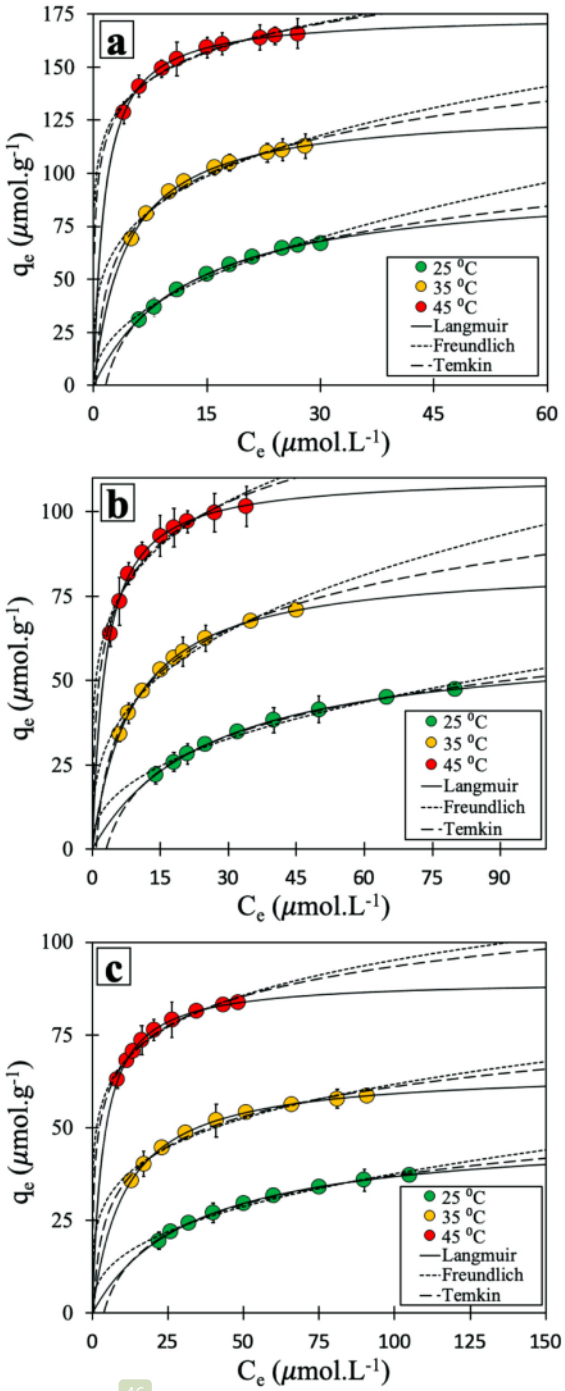

Fig. 5. Isotherm experimental data fitted with the Langmuir, the Freundlich and the Temkin isotherm models for magnetic clean-up of BF (a), MV (b) and MG (c) at temperature 25 °C, 35 °C and 45 °C by $CoFe_2O_4$-HA-ECH (experiment condition: pH 7, adsorbent dose: 2 g.L^{-1}, t: 2 h, n: 3).

$$q_e = \frac{q_{max} \bullet K_L \bullet C_e}{1 + (K_L \bullet C_e)} \quad (9)$$

Table 2
Magnetic removal kinetics parameters of BF, MV and MG by $CoFe_2O_4$, $CoFe_2O_4$-HA and $CoFe_2O_4$-HA-ECH obtained from non-linearized pseudo-first order (PFO), pseudo-second order (PSO) and Elovich kinetics model.

Kinetics	Parameter	$CoFe_2O_4$			$CoFe_2O_4$-HA			$CoFe_2O_4$-HA-ECH		
		BF	MV	MG	BF	MV	MG	BF	MV	MG
PFO	q_e[a]	7.587	4.865	3.015	56.255	39.235	27.517	81.777	49.235	39.504
	K_{PFO}[b]	0.047	0.037	0.019	0.184	0.116	0.108	0.159	0.110	0.067
	R^2	0.997	0.997	0.996	0.989	0.984	0.982	0.989	0.988	0.993
	χ^2	0.133	0.148	0.379	1.188	1.942	1.976	2.142	1.496	0.784
	ARE	3.651	5.762	9.694	5.931	9.441	5.593	6.866	8.049	7.913
PSO	q_e[a]	9.976	6.684	4.273	61.772	44.286	36.714	90.241	58.334	46.751
	K_{PSO}[c]	4.14×10^{-3}	4.47×10^{-3}	3.51×10^{-3}	3.73×10^{-3}	3.01×10^{-3}	2.44×10^{-3}	2.15×10^{-3}	1.98×10^{-3}	1.503×10^{-3}
	R^2	0.998	0.999	0.999	0.999	0.998	1.000	1.000	0.999	1.000
	χ^2	0.131	0.106	0.298	0.171	0.165	0.065	0.005	0.063	0.023
	ARE	2.775	3.012	3.443	2.019	2.952	2.571	0.292	1.214	1.321
Elovich	α[d]	0.550	0.238	0.071	36.323	10.637	5.060	39.148	11.326	4.625
	β[e]	0.403	0.510	0.694	0.093	0.111	0.120	0.060	0.081	0.089
	R^2	0.992	0.994	0.995	0.968	0.989	0.988	0.977	0.986	0.991
	χ^2	0.343	0.281	0.331	3.826	1.164	1.134	3.988	1.637	1.043
	ARE	5.497	8.963	7.763	11.596	8.878	4.870	10.126	9.170	10.569

[a] q_e in μmol $\cdot g^{-1}$.
[b] K_{PFO} in min^{-1}.
[c] K_{PSO} in g$\cdot$ μmol $^{-1}\cdot min^{-1}$.
[d] α in μmol. g^{-1}. min^{-1}.
[e] β in g$\cdot$ μmol $^{-1}$.

$$q_e = q_{max} \ln(K_T . C_e) \quad (10)$$

where q_e and q_{max} are the amounts of removed dyes at equilibrium (μmol. g^{-1}) and the maximum adsorption capacity of the adsorbents (μmol. g^{-1}), respectively; C_e is the remaining concentration of the dyes in bulk solution at equilibrium (μmol.L^{-1}); 1/n is the non-dimensional Freundlich isotherm parameter associated with the binding affinity of the adsorbents with the dyes; and K_F, K_L, and K_T are the Freundlich ((μmol $\cdot g^{-1}$)(L$\cdot$ μmol^{-1})$^{1/n}$), Langmuir (L. μmol^{-1}), and Temkin isotherm constants (L. g^{-1}), respectively. The Freundlich isotherm model describes adsorbate-adsorbate interactions on the surface of an adsorbent with multilayer coverage. The Freundlich isotherm assumes that the surface of the adsorbent is heterogenous and has different levels of bond energy. The adsorbate will attach to adsorbent surfaces with higher bond energies before attaching to surfaces with lower bond energies [53]. In contrast, the Langmuir isotherm model was developed for adsorbents with a homogenous surface. Adsorbate is adsorbed on the surface of the adsorbent as a monolayer without any interaction between adsorbates [54]. According to the Temkin isotherm model, the adsorption energy of all adsorbates in a layer declines linearly rather than logarithmically and it takes into account adsorbate-adsorbate interactions. [55].

The adsorption isotherm results generated by evaluating experimental data with these three models are presented in Fig. 5 and all estimated parameters are listed in Table 3. As shown in Fig. 5, simulating the experimental data with the non-linearized Langmuir curves shows an excellent fit, better than those with the non-linearized Freundlich and Temkin models, indicating monolayer formation of BF, MV, and MG on a homogenous surface of $CoFe_2O_4$-HA-ECH. Higher R^2 values ($\geq$ 0.999) and lower χ^2 ($\leq$ 0.025) and ARE ($\leq$ 0.891) values indicate that all experimental data fitted well with the Langmuir isotherm models. Moreover, the q_{max} values calculated from the non-linear Langmuir isotherm (Table 3) were in good agreement with the q_e values obtained from the PSO kinetics model (Table 2). The q_{max} for BF, MV, and MG by adsorbents all followed the order $CoFe_2O_4$-HA-ECH > $CoFe_2O_4$-HA > $CoFe_2O_4$. Moreover, $CoFe_2O_4$-HA-ECH has a higher q_{max} value than $CoFe_2O_4$-HA, probably due to the presence of the higher number of the crosslinked HA layer that produces more active adsorption sites and more negative surfaces as confirmed by TGA (Fig. 2b) and ζ-potential analyses (Fig. 3a). The $CoFe_2O_4$ itself barely adsorbs the dyes but it contributes to the magnetic properties of $CoFe_2O_4$-HA-ECH and $CoFe_2O_4$-HA so that $CoFe_2O_4$-HA-ECH and $CoFe_2O_4$-HA can be separated easily by using an external magnet.

The isotherm curves (Fig. 5) can be used to predict the dye adsorption mechanism by $CoFe_2O_4$-HA-ECH. Giles et al. classified the shapes of isotherm curves into four main classes, namely S, L, H, and C [56]. The isotherm curves of $CoFe_2O_4$-HA-ECH fall into the L class which indicates that solvent does not compete with the dyes to occupy the active sites of $CoFe_2O_4$-HA-ECH. Similar phenomena were observed for removal of Congo Red from solution by cationic surfactant-modified tea waste [57].

3.5. Temperature dependent adsorption and thermodynamics study

In order to obtain more detailed evidence of the mechanism taking place on the surface of $CoFe_2O_4$-HA-ECH during the adsorption of the dyes, thermodynamic experiments were conducted at various temperatures from 25 to 45 °C, and the results are presented in Fig. 5. The q_{max} value increased as the temperature increased, which indicates that removal of the dyes by the adsorbents is favorable at higher temperatures. Higher temperature not only increases the mobility of adsorbate in the solution but also intensifies the adsorbent-adsorbate collisions, leading to higher removal efficiency.

The experimental data were further used to determine Gibbs free energy (ΔG^0, kJ. mol^{-1}), changes of enthalpy (ΔH^0, kJ. mol^{-1}), and changes of entropy (ΔS^0, J. $mol^{-1}.K^{-1}$) by using the following equations:

$$\Delta G^0 = -RTLn(K_e^0) \quad (11)$$

$$\Delta G^0 = \Delta H^0 - T . \Delta S^0 \quad (12)$$

where ΔG^0 is the Gibbs free energy (kJ. mol^{-1}), R is the universal gas constant (8.314 J.K^{-1}. mol^{-1}), T is the temperature (K), and ΔH^0 and ΔS^0 are the changes of enthalpy (kJ. mol^{-1}) and entropy (J. $mol^{-1}.K^{-1}$). The thermodynamic equilibrium constant (K_e^0) can be determined by using the following formula:

$$K_e^0 = \frac{10^6 . K_L . [Dye]^0}{\gamma} \quad (13)$$

where K_L is the Langmuir isotherm constant (L. μmol^{-1}), $[Dye]^0$ is the standard concentration of the dye, and γ is the coefficient of activity [58]. By combining Eq. (11) and Eq. (12), ΔH^0 and ΔS^0 can be

Table 3
The Freundlich, Langmuir and Temkin isotherm parameters for magnetic removal of BF, MV and MG by $CoFe_2O_4$, $CoFe_2O_4$-HA and $CoFe_2O_4$-HA-ECH at various temperatures.

T (°C)	Isotherm	Parameter	$CoFe_2O_4$			$CoFe_2O_4$-HA			$CoFe_2O_4$-HA-ECH		
			BF	MV	MG	BF	MV	MG	BF	MV	MG
25	Freundlich	1/n	0.382	0.457	0.559	0.376	0.368	0.367	0.457	0.411	0.388
		K_F [a]	0.942	0.398	0.123	9.255	6.412	4.747	14.748	8.091	6.289
		R^2	0.980	0.980	0.993	0.983	0.979	0.982	0.983	0.981	0.984
		χ^2	0.053	0.051	0.013	0.247	0.344	0.193	0.491	0.365	0.190
		ARE	2.709	3.348	2.275	2.086	2.999	2.659	2.994	2.994	2.323
	Langmuir	q_{max} [b]	9.762	6.801	4.317	66.161	47.839	37.324	96.492	62.627	48.740
		K_L [c]	0.014	0.010	0.006	0.034	0.029	0.024	0.079	0.039	0.031
		R^2	1.000	0.999	1.000	0.999	0.999	1.000	0.999	1.000	1.000
		χ^2	7.79×10^{-4}	4.19×10^{-3}	2.25×10^{-3}	9.05×10^{-3}	0.023	3.769×10^{-3}	0.025	1.464×10^{-3}	6.68×10^{-3}
		ARE	0.302	0.891	0.332	0.374	0.557	0.373	0.583	0.177	0.363
	Temkin	q_{max} [b]	0.901	1.637	0.999	15.203	10.795	8.442	23.219	14.747	11.345
		K_T [d]	4.324	0.078	0.054	0.298	0.262	0.220	0.632	0.324	0.264
		R^2	0.997	0.999	0.997	0.998	0.996	0.998	0.998	0.998	0.998
		χ^2	7.567	0.003	0.005	0.032	0.049	0.022	0.051	0.027	0.024
		ARE	21.625	0.874	1.583	0.805	1.054	0.915	0.801	0.813	0.837
35	Freundlich	1/n	0.254	0.327	0.406	0.276	0.234	0.229	0.258	0.331	0.233
		K_F [a]	2.454	1.118	0.450	22.098	16.496	13.240	49.010	20.937	21.141
		R^2	0.974	0.977	0.985	0.982	0.982	0.973	0.964	0.966	0.961
		χ^2	0.034	0.047	0.023	0.115	0.138	0.167	0.731	0.850	0.448
		ARE	1.822	2.673	2.367	1.301	1.546	1.946	2.450	3.812	2.868
	Langmuir	q_{max} [b]	11.060	7.909	5.428	79.747	54.649	44.611	130.442	84.786	65.531
		K_L [c]	0.027	0.020	0.012	0.085	0.071	0.060	0.230	0.112	0.093
		R^2	1.000	0.999	0.999	0.999	0.999	0.999	0.999	1.000	1.000
		χ^2	2×10^{-3}	2.57×10^{-3}	1.82×10^{-3}	3.89×10^{-3}	0.0202	9.39×10^{-3}	0.015	1.18×10^{-3}	1.22×10^{-3}
		ARE	0.090	0.501	0.649	0.210	0.553	0.432	0.328	0.115	0.123
	Temkin	q_{max} [b]	2.084	1.702	1.266	15.886	9.656	7.799	24.848	18.468	11.617
		K_T [d]	0.458	0.206	0.106	1.191	1.495	1.318	3.654	1.133	1.916
		R^2	0.989	0.995	0.998	0.993	0.993	0.989	0.984	0.993	0.981
		χ^2	0.014	0.010	0.003	0.047	0.052	0.065	0.326	0.160	0.208
		ARE	1.204	1.300	0.779	0.864	0.981	1.231	1.728	1.647	1.934
45	Freundlich	1/n	0.153	0.216	0.278	0.150	0.133	0.145	0.124	0.200	0.152
		K_F [a]	4.838	2.538	1.169	49.268	34.076	26.326	72.148	52.337	47.283
		R^2	0.974	0.956	0.975	0.983	0.949	0.964	0.957	0.940	0.966
		χ^2	0.016	0.060	0.028	0.050	0.170	0.142	0.371	0.965	0.195
		ARE	1.128	2.650	2.224	0.704	1.519	1.569	1.451	3.201	1.486
	Langmuir	q_{max} [b]	11.780	8.880	6.079	95.663	64.980	54.160	174.516	110.794	89.936
		K_L [c]	0.056	0.040	0.025	0.215	0.178	0.147	0.692	0.340	0.275
		R^2	0.999	1.000	0.999	1.000	0.998	0.999	0.999	0.999	1.000
		χ^2	8.06×10^{-4}	1.48×10^{-3}	1.83×10^{-3}	1.39×10^{-3}	5.93×10^{-3}	4.27×10^{-3}	0.011	0.021	2.19×10^{-3}
		ARE	0.229	0.247	0.414	0.104	0.242	0.256	0.215	0.380	0.134
	Temkin	q_{max} [b]	1.526	1.496	1.201	12.176	7.482	6.679	18.983	17.723	11.586
		K_T [d]	6.250	1.027	0.345	28.347	43.681	21.455	64.679	11.073	31.810
		R^2	0.984	0.978	0.992	0.989	0.961	0.977	0.970	0.966	0.978
		χ^2	0.010	0.030	0.009	0.032	0.128	0.090	0.261	0.541	0.125
		ARE	0.897	1.909	1.300	0.564	1.320	1.264	1.248	2.401	1.193

[a] K_F in $(\mu mol \cdot g^{-1})(L \cdot \mu mol^{-1})^{1/n}$.
[b] q_{max} in $\mu mol \cdot g^{-1}$.
[c] K_L in $L \cdot \mu mol^{-1}$.
[d] K_T in $L \cdot \mu mol^{-1}$.

determined from:

$$Ln(K_e^0) = -\frac{\Delta H^0}{R} \cdot \frac{1}{T} + \frac{\Delta S^0}{R} \quad (14)$$

Van't Hoff plots (Ln (K_e^0) vs 1/T) were used to estimate ΔH^0 and ΔS^0, and are shown in Fig. 6. The estimated thermodynamics parameters (ΔG^0, ΔH^0, and ΔS^0) are listed in Table 4. Negative ΔG^0 values indicate removal of dyes by the adsorbents are spontaneous reactions and favorable mechanisms at higher temperature. Positive values of ΔH^0 at increasing temperature indicate that removal of dye is an endothermic process. Higher enthalpy between dyes and adsorbents during the adsorption process at all ranges of studied temperature are indicated by positive values of ΔS^0. It can be concluded that temperature plays an important role for the removal of BF, MV, and MG by $CoFe_2O_4$, $CoFe_2O_4$-HA and $CoFe_2O_4$-HA-ECH.

3.6. Performance evaluation

The effect of ionic strength on the removal of the dyes with the adsorbents was explored at different NaCl concentrations. As shown in Fig. 7(a–c), the amount of adsorbed dyes on the surface of the adsorbents decreases as the concentration of NaCl increases. The presence of NaCl in the solution diminishes electrostatic interaction between positively charged dye molecules with negatively charged adsorbents, due to a competition effect. Also, increased ionic strength limits the mobility of dye molecules in solution to approach the active adsorption sites.

From an economic point of view, the regeneration and reusability of the adsorbents is essential, due to their high q_{max} values, rapid removal kinetics, and high saturation magnetization. At the end of the removal experiments, adsorbents loaded with dyes were dispersed in 20 ml of 10 wt.% NaCl in 25 % acetic acid solution and stirred for 25 min to detach the dye molecules, rinsed with ethanol, dried in the oven and

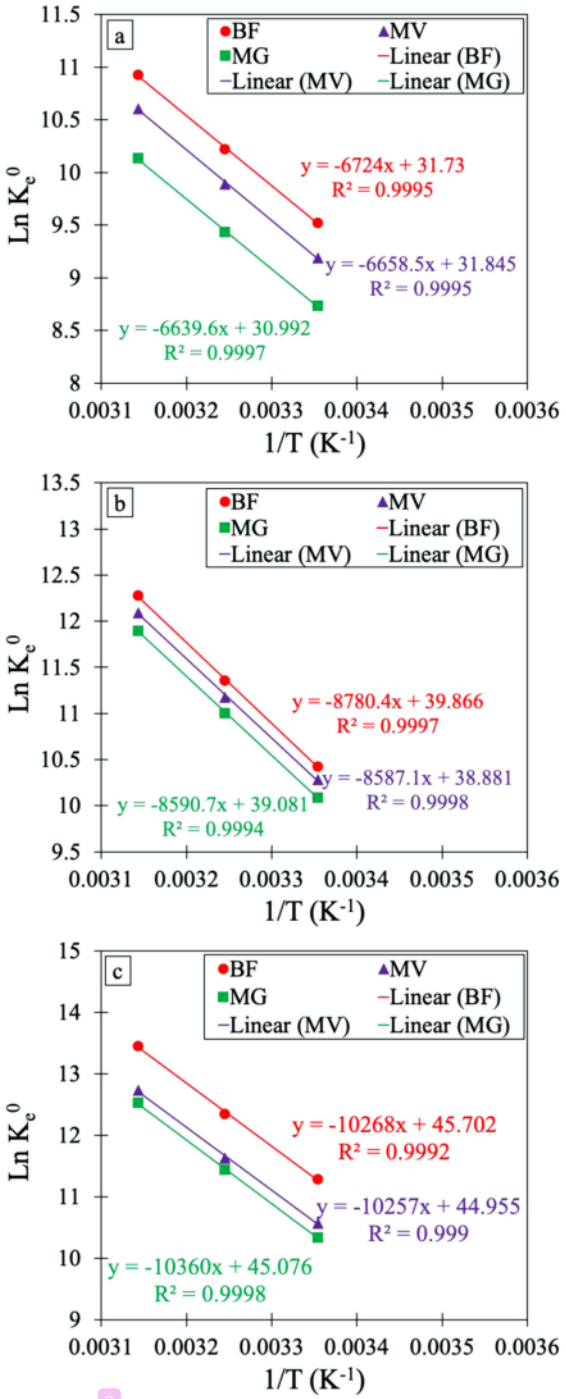

Fig. 6. Plot of Van't Hoff for magnetic removal of BF, MV, and MG by $CoFe_2O_4$ (a), $CoFe_2O_4$-HA (b) and $CoFe_2O_4$-HA-ECH (c).

further used for the next cycle of dye removal. As illustrated in Fig. 7(d–f), the $CoFe_2O_4$ lost more than 50 % of its adsorptive performance for the dyes after 10 cycles while $CoFe_2O_4$-HA-ECH lost no more than 3% from its initial performance, which is a minor performance drop compared to that of $CoFe_2O_4$-HA. The crosslinked HA layers on the surface of $CoFe_2O_4$-HA-ECH are more stable than the non-crosslinked HA on the surface of $CoFe_2O_4$-HA. Therefore, $CoFe_2O_4$-HA-ECH did not loss its adsorptive performance significantly. The results show that $CoFe_2O_4$-HA-ECH exhibits high stability and recyclability, although it is affected by the ionic strength of solution.

To evaluate the performance of the as-prepared adsorbents for the removal of BF, MV, and MG, the obtained q_{max}, adsorption rate, and Ms values were compared to those of adsorbents in other published works. Table 5 reveals that $CoFe_2O_4$-HA-ECH has higher q_{max} values for BF, MV, and MG than some adsorbents reported elsewhere [47–49,59–63]. Some previously reported adsorbents show higher q_{max} than $CoFe_2O_4$-HA-ECH. However, those materials require longer times and exhibit lower Ms values. The removal process using $CoFe_2O_4$-HA-ECH only requires a short time, indicating a rapid removal process, which would minimize the cost of a large-scale application. Furthermore, its high q_{max} values, rapid removal kinetics, and easy re-collection with an external magnet make $CoFe_2O_4$-HA-ECH a good prospect for use in commercial applications.

4. Conclusions

In this study, spinel cobalt ferrite ($CoFe_2O_4$) was successfully functionalized with humic acid ($CoFe_2O_4$-HA) and epichlorohydrin-crosslinked humic acid ($CoFe_2O_4$-HA-ECH) by a hydrothermal method. Epichlorohydrin was used as a crosslinking agent to avoid detachment of the HA layer on the surface of $CoFe_2O_4$. The physicochemical properties of $CoFe_2O_4$, $CoFe_2O_4$-HA, and $CoFe_2O_4$-HA-ECH were characterized by PSA, SEM, FTIR, TGA, XRD, VSM, and ζ-potential analysis. PSA and SEM analyses showed that the average adsorbent particle size ranges from 37.85 to 80.73 μm and that the particles have an irregular shape and a rough surface. The presence of HA and crosslinked HA was detected through FTIR and TGA. X-ray diffractograms confirmed the presence of the pure cubic phase of $CoFe_2O_4$. The VSM results showed that the saturation magnetization values of $CoFe_2O_4$, $CoFe_2O_4$-HA, and $CoFe_2O_4$-HA-ECH are 56.408, 49.233, and 34.009 $emu.g^{-1}$, respectively, indicating that these adsorbents can be separated easily with a magnet. ζ-potential analyses showed that $CoFe_2O_4$-HA-ECH is negatively charged over the entire range of pH studied, and its interaction with BF, MV, and MG was dominated by the electrostatic interaction. Kinetic studies revealed that the adsorption processes were very fast with an equilibrium time of 30 min, and followed a pseudo second order model with $R^2 \geq 0.998$, $\chi^2 \leq 0.171$, and ARE ≤ 3.443. The q_{max} values of $CoFe_2O_4$-HA-ECH were 96.492, 62.627, and 48.740 $\mu mol \cdot g^{-1}$ for BF, MV, and MG, respectively, which are considerably higher than those of $CoFe_2O_4$ and $CoFe_2O_4$-HA. Isotherm modelling demonstrated that removal of BF, MV, and MG fit with the Langmuir isotherm model with $R^2 \geq 0.999$, $\chi^2 \leq 0.025$, and ARE ≤ 0.891. The calculated thermodynamic parameters revealed that the adsorption processes are spontaneous and endothermic. A recycling process was successfully performed and the adsorptive performance of the obtained adsorbents could be retained even after the 10th cycle.

CRediT authorship contribution statement

Satya Candra Wibawa Sakti: Conceptualization, Methodology, Investigation, Writing - original draft. **Rahma Nuzulul Laily:** Investigation. **Siti Aliyah:** Investigation. **Nindayu Indrasari:** Investigation. **Mochamad Zakki Fahmi:** Investigation, Writing - review & editing. **Hwei Voon Lee:** Investigation, Writing - review & editing. **Yasuhiro Akemoto:** Investigation. **Shunitz Tanaka:** Conceptualization.

Table 4
Thermodynamic parameters for magnetic removal of BF, MV and MG by $CoFe_2O_4$, $CoFe_2O_4$-HA and $CoFe_2O_4$-HA-ECH.

Adsorbate	T (K)	$CoFe_2O_4$				$CoFe_2O_4$-HA				$CoFe_2O_4$-HA-ECH			
		Ln K_e^0	$\Delta G^{0,a}$	$\Delta H^{0,b}$	$\Delta S^{0,c}$	Ln K_e^0	$\Delta G^{0,a}$	$\Delta H^{0,b}$	$\Delta S^{0,c}$	Ln K_e^0	$\Delta G^{0,a}$	$\Delta H^{0,b}$	$\Delta S^{0,c}$
BF	298.15	9.521	−23.580	55.359	264.760	10.425	−25.820	73.001	331.447	11.281	−27.921	85.367	379.970
	308.15	10.220	−26.227			11.355	−29.135			12.347	−31.721		
	318.15	10.925	−28.875			12.277	−32.449			13.447	−35.521		
MV	298.15	9.186	−22.749	55.904	263.802	10.280	−25.452	71.423	324.921	10.571	−26.157	85.279	373.756
	308.15	9.891	−25.387			11.177	−28.701			11.629	−29.894		
	318.15	10.604	−28.025			12.092	−31.950			12.735	−33.632		
MG	298.15	8.730	−21.622	55.202	257.670	10.086	−24.985	71.393	323.253	10.339	−25.605	86.130	374.762
	308.15	9.431	−24.199			11.001	−28.217			11.438	−29.353		
	318.15	10.130	−26.776			11.897	−31.450			12.524	−33.101		

[a] ΔG^0 in kJ. mol^{-1}.
[b] ΔH^0 in kJ. mol^{-1}.
[c] ΔS^0 in J. mol^{-1}. K^{-1}.

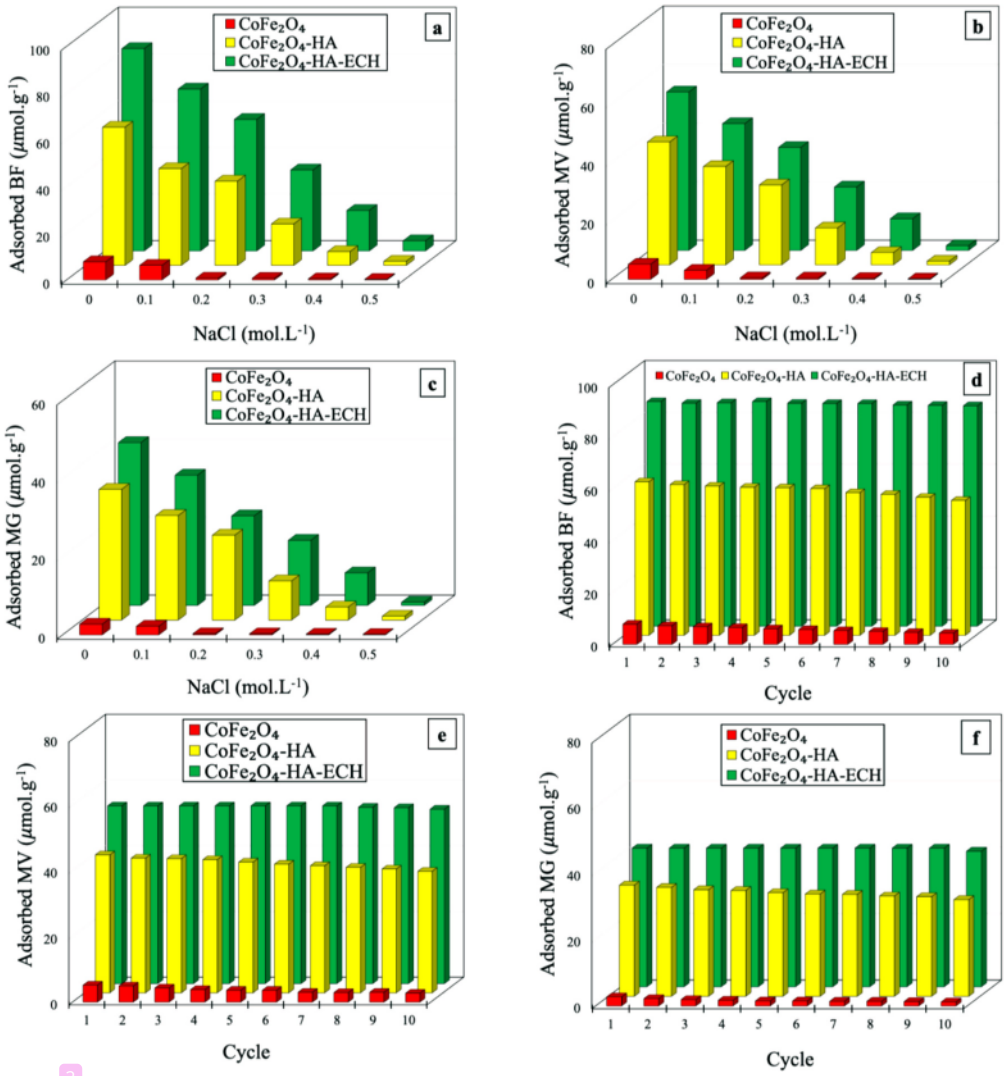

Fig. 7. Effect of NaCl on magnetic removal of BF (a), MV (b), MG (c) by $CoFe_2O_4$, $CoFe_2O_4$-HA, $CoFe_2O_4$-HA-ECH and recyclability of $CoFe_2O_4$, $CoFe_2O_4$-HA, $CoFe_2O_4$-HA-ECH during 10 consecutive magnetic removal cycles of BF (d), MV (e) and MG (f).

Table 5
Removal performance comparison with other magnetic adsorbents.

Magnetic Adsorbent	t_{eq} (min)	q_{max} (mg. g^{-1})			Ms (emu. g^{-1})	Ref.
		BF	MV	MG		
Activated carbon/ferrospinel composite	30	101	–	–	na	[47]
$MgFe_2O_4$ nanoparticle	30	1.231	–	–	28.5	[48]
SDS-coated Fe_3O_4 nanoparticle	20	–	416.7	–	na	[49]
Algal activated carbon/Fe_3O_4 magnetic composite	30	–	59.88	–	26.57	[59]
3D porous ferromagnetic $NiFe_2O_4$	90	–	19.06	–	15.04	[60]
Fe_3O_4/Persimmon tannins/GO	240	–	–	558.66	22.2	[61]
$Ba_3(PO_4)_2/Fe_3O_4$	120	–	–	1639	0.87	[62]
$CoFe_2O_4$-polydopamine-alginate bead	500	–	–	248.78	23.85	[63]
$CoFe_2O_4$	30	3.16	2.68	2.00	56.41	this work
$CoFe_2O_4$-HA	30	21.42	18.85	17.30	49.23	this work
$CoFe_2O_4$-HA-ECH	30	31.25	24.67	22.59	34.01	this work

Declaration of Competing Interest

The authors declare that they have no known competing financial interest or personal relationship that could have appeared to influence the work reported in this paper.

Acknowledgements

The authors sincerely acknowledge financial support from Faculty of Science and Technology, Universitas Airlangga, Indonesia with contract number 3198/UN3.1.8/LT/2017. ξ-potentials and scanning electron microscopy analyses were carried out at Creative Research Institution (CRIS), Hokkaido University, Japan. Particle size measurements were performed at Laboratory of Nano-Micro Material Analysis, Material Analysis and Structure Analysis Open Unit (MASAOU), Hokkaido University, Japan. Vibrating Sample Magnetometry analyses were conducted at Nanotechnology and Catalysis Research Centre, University of Malaya, Malaysia.

References

[1] T.K. Sen, S. Afroze, H.M. Ang, Equilibrium, kinetics and mechanism of removal of methylene blue from aqueous solution by adsorption onto pine cone biomass of Pinus radiata, Water Air Soil Pollut. 218 (2011) 499–515, https://doi.org/10.1007/s11270-010-0663-y.
[2] A. Ajmal, I. Majeed, R.N. Malik, H. Idriss, M.A. Nadeem, Principles and mechanisms of photocatalytic dye degradation on TiO_2 based photocatalysts: a comparative overview, RSC Adv. 4 (2014) 37003–37026, https://doi.org/10.1039/c4ra06658h.
[3] A. Tkaczyk, K. Mitrowska, A. Posyniak, Synthetic organic dyes as contaminants of the aquatic environment and their implications for ecosystems : a review, Sci. Total Environ. 717 (2020) 137222, , https://doi.org/10.1016/j.scitotenv.2020.137222.
[4] L. Ayed, K. Bakir, H. Ben, S. Hammami, Microbial pathogenesis in vitro mutagenicity, NMR metabolite characterization of azo and triphenylmethanes dyes by adherents bacteria and the role of the "cna" adhesion gene in activated sludge, Microb. Pathog. 103 (2017) 29–39, https://doi.org/10.1016/j.micpath.2016.12.016.
[5] V.K. Balakrishnan, S. Shirin, A.M. Aman, S.R. de Solla, J. Mathieu-Denoncourt, V.S. Langlois, Genotoxic and carcinogenic products arising from reductive transformations of the azo dye, disperse yellow 7, Chemosphere 146 (2016) 206–215, https://doi.org/10.1016/j.chemosphere.2015.11.119.
[6] D.F. Duxbury, The photochemistry and photophysics of triphenylmethane dyes in solid and liquid media, Chem. Rev. 93 (1993) 381–433, https://doi.org/10.1021/cr00017a018.
[7] K. Venkataraman, The Chemistry of Synthetic Dyes, Academic press, New York, USA, 2012.
[8] V. Katheresan, J. Kansedo, S.Y. Lau, Efficiency of various recent wastewater dye removal methods: a review, J. Environ. Chem. Eng. 6 (2018) 4676–4697, https://doi.org/10.1016/j.jece.2018.06.060.
[9] K. Vikrant, B.S. Giri, N. Raza, K. Roy, K.H. Kim, B.N. Rai, R.S. Singh, Recent advancements in bioremediation of dye: current status and challenges, Bioresour. Technol. 253 (2018) 355–367, https://doi.org/10.1016/j.biortech.2018.01.029.
[10] M.T. Yagub, T.K. Sen, S. Afroze, H.M. Ang, Dye and its removal from aqueous solution by adsorption: a review, Adv. Colloid Interface Sci. 209 (2014) 172–184, https://doi.org/10.1016/j.cis.2014.04.002.
[11] E.S. Mansor, H. Abdallah, A.M. Shaban, Fabrication of high selectivity blend membranes based on poly vinyl alcohol for crystal violet dye removal, J. Environ. Chem. Eng. (2020) 103706, https://doi.org/10.1016/j.jece.2020.103706.
[12] C.N.C. Hitam, A.A. Jalil, A review on exploration of Fe_2O_3 photocatalyst towards degradation of dyes and organic contaminants, J. Environ. Manage. 258 (2020) 110050, , https://doi.org/10.1016/j.jenvman.2019.110050.
[13] N. De Camargo, L. Beluci, G. Affonso, P. Mateus, C. Sayury, N. Cândido, R. Guttierres, M.R. Fagundes-klen, R. Bergamasco, A. Marquetotti, S. Vieira, Hybrid treatment of coagulation/flocculation process followed by ultra filtration in TiO_2 -modified membranes to improve the removal of reactive black 5 dye, Sci. Total Environ. 664 (2019) 222–229, https://doi.org/10.1016/j.scitotenv.2019.01.199.
[14] A.C.N. Pinheiro, T.S. Bernardino, F.E.B. Junior, M.R.V. Lanza, W.R.P. Barros, Enhanced electrodegradation of the sunset yellow dye in acid media by heterogeneous photoelectro-fenton process using Fe_3O_4 nanoparticles as a catalyst, J. Environ. Chem. Eng. 8 (2020) 103621, , https://doi.org/10.1016/j.jece.2019.103621.
[15] A. Das, S. Mishra, Removal of textile dye reactive green-19 using bacterial consortium: process optimization using response surface methodology and kinetics study, J. Environ. Chem. Eng. 5 (2017) 612–627, https://doi.org/10.1016/j.jece.2016.10.005.
[16] A. Afkhami, S. Sayari, R. Moosavi, T. Madrakian, Magnetic nickel zinc ferrite nanocomposite as an efficient adsorbent for the removal of organic dyes from aqueous solutions, J. Ind. Eng. Chem. 21 (2015) 920–924, https://doi.org/10.1016/j.jiec.2014.04.033.
[17] T. Madrakian, A. Afkhami, M. Ahmadi, Adsorption and kinetic studies of seven different organic dyes onto magnetite nanoparticles loaded tea waste and removal of them from wastewater samples, Spectrochim. Acta - Part A Mol. Biomol. Spectrosc. 99 (2012) 102–109, https://doi.org/10.1016/j.saa.2012.09.025.
[18] T. Madrakian, A. Afkhami, R. Haryani, M. Ahmadi, Synthesis of g-Fe_2O_3/TiO_2 nanocomposite and its application in removal of dyes from water samples by adsorption and degradation processes, RSC Adv. 4 (2014) 44841–44847, https://doi.org/10.1039/C4RA06421F.
[19] A. Ibanescu, M.C. Alexandrica, D. Hritcu, O. Chiscan, M.I. Popa, Magnetite/chitosan composite particles as adsorbents for Reactive Blue 19 dye, Int. J. Green Nanotechnol. Mater. Sci. Eng. 6 (2018) 149–156, https://doi.org/10.1680/jgrma.18.00039.
[20] M.L. Iordache, G. Dodi, D. Hritcu, D. Draganescu, O. Chiscan, M.I. Popa, Magnetic chitosan grafted (alkyl acrylate) composite particles: synthesis, characterization and evaluation as adsorbents, Arab. J. Chem. 11 (2018) 1032–1043, https://doi.org/10.1016/j.arabjc.2015.12.010.
[21] B.A.G. de Melo, F.L. Motta, M.H.A. Santana, Humic acids: structural properties and multiple functionalities for novel technological developments, Mater. Sci. Eng. C. 62 (2015) 967–974, https://doi.org/10.1016/j.msec.2015.12.001.
[22] W.W. Tang, G.M. Zeng, J.L. Gong, J. Liang, P. Xu, C. Zhang, B. Bin Huang, Impact of humic/fulvic acid on the removal of heavy metals from aqueous solutions using nanomaterials: a review, Sci. Total Environ. 468–469 (2014) 1014–1027, https://doi.org/10.1016/j.scitotenv.2013.09.044.
[23] S. Lu, W. Liu, Y. Wang, Y. Zhang, P. Li, D. Jiang, C. Fang, Y. Li, An adsorbent based on humic acid and carboxymethyl cellulose for efficient dye removal from aqueous solution, Int. J. Biol. Macromol. 135 (2019) 790–797, https://doi.org/10.1016/j.ijbiomac.2019.05.095.
[24] H. Yang, J. Gong, G. Zeng, P. Zhang, J. Zhang, H. Liu, Polyurethane foam membranes filled with humic acid-chitosan crosslinked gels for selective and simultaneous removal of dyes, J. Colloid Interface Sci. 505 (2017) 67–78, https://doi.org/10.1016/j.jcis.2017.05.075.
[25] H. Basu, S. Saha, I.A. Mahadevan, M.V. Pimple, Humic acid coated cellulose derived from rice husk : a novel biosorbent for the removal of Ni and Cr, J. Water Process Eng. 32 (2019) 100892, , https://doi.org/10.1016/j.jwpe.2019.100892.
[26] A.B. Volikov, S.A. Ponomarenko, A.I. Konstantinov, K. Hat, I.V. Perminova, Nature-like solution for removal of direct brown 1 azo dye from aqueous phase using humics-modified silica gel, Chemosphere 145 (2016) 83–88, https://doi.org/10.1016/j.chemosphere.2015.11.070.
[27] C. Yang, Q. Zeng, Y. Yang, R. Xiao, Chemistry the synthesis of humic acids graft copolymer and its adsorption for organic pesticides, J. Ind. Eng. Chem. 20 (2014) 1133–1139.
[28] K.K. Kefeni, T.A.M. Msagati, T. Ti, B.B. Mamba, Spinel ferrite nanoparticles and nanocomposites for biomedical applications and their toxicity, Mater. Sci. Eng. C.

107 (2020) 110314, , https://doi.org/10.1016/j.msec.2019.110314.
[29] K.K. Kefeni, B.B. Mamba, T.A.M. Msagati, Application of spinel ferrite nanoparticles in water and wastewater treatment : a review tetrahedral site octahedral site oxygen, Sep. Purif. Technol. 188 (2017) 399–422, https://doi.org/10.1016/j.seppur.2017.07.015.
[30] M. Houshiar, F. Zebhi, Z.J. Razi, A. Alidoust, Z. Askari, Synthesis of cobalt ferrite ($CoFe_2O_4$) nanoparticles using combustion, coprecipitation, and precipitation methods: a comparison study of size, structural, and magnetic properties, J. Magn. Magn. Mater. 371 (2014) 43–48, https://doi.org/10.1016/j.jmmm.2014.06.059.
[31] A. Mazrouei, A. Saidi, Microstructure and magnetic properties of cobalt ferrite nano powder prepared by solution combustion synthesis, Mater. Chem. Phys. 209 (2018) 152–158, https://doi.org/10.1016/j.matchemphys.2018.01.075.
[32] M. Shyamalsas, C. Bououdina, Manoharan, Dependence of structure/morphology on electrical/magnetic properties of hydrothermally synthesised cobalt ferrite nanoparticles, J. Magn. Magn. Mater. 493 (2020) 165703, , https://doi.org/10.1016/j.jmmm.2019.165703.
[33] M.A. Almessiere, Y. Slimani, A.D. Korkmaz, S. Guner, M. Sertkol, S.E. Shirsath, A. Baykal, Structural, optical and magnetic properties of Tm^{3+} substituted cobalt spinel ferrites synthesized via sonochemical approach, Ultrason. - Sonochemistry. 54 (2019) 1–10, https://doi.org/10.1016/j.ultsonch.2019.02.022.
[34] J. Venturini, T.B. Wermuth, M.C. Machado, S. Arcaro, A.K. Alves, A. da Cas Viegas, C.P. Bergmann, The influence of solvent composition in the sol-gel synthesis of cobalt ferrite ($CoFe_2O_4$): a route to tuning its magnetic and mechanical properties, J. Eur. Ceram. Soc. 39 (2019) 3442–3449, https://doi.org/10.1016/j.jeurceramsoc.2019.01.030.
[35] D.H.K. Reddy, Y.S. Yun, Spinel ferrite magnetic adsorbents: alternative future materials for water purification, Coord. Chem. Rev. 315 (2016) 90–111, https://doi.org/10.1016/j.ccr.2016.01.012.
[36] S. Jovanović, M. Spreitzer, M. Otoničar, J.-H. Jeon, D. Suvorov, pH control of magnetic properties in precipitation-hydrothermal-derived $CoFe_2O_4$, J. Alloys. Compd. 589 (2014) 271–277, https://doi.org/10.1016/j.jallcom.2013.11.217.
[37] K.L. Routray, S. Saha, D. Behera, Green synthesis approach for nano sized CoFe2O4 through aloe vera mediated sol-gel auto combustion method for high frequency devices, Mater. Chem. Phys. 224 (2019) 29–35, https://doi.org/10.1016/j.matchemphys.2018.11.073.
[38] M. Houshiar, F. Zebhi, Z.J. Razi, A. Alidoust, Z. Askari, Synthesis of cobalt ferrite ($CoFe_2O_4$) nanoparticles using combustion, coprecipitation, and precipitation methods: a comparison study of size, structural, and magnetic properties, J. Magn. Magn. Mater. 371 (2014) 43–48, https://doi.org/10.1016/j.jmmm.2014.06.059.
[39] B. Paul, D.D. Purkayastha, S.S. Dhar, One-pot hydrothermal synthesis and characterization of $CoFe_2O_4$ nanoparticles and its application as magnetically recoverable catalyst in oxidation of alcohols by periodic acid, Mater. Chem. Phys. 181 (2016) 99–105, https://doi.org/10.1016/j.matchemphys.2016.06.039.
[40] D. Hu, F. Zhao, Z. Zhang, L. Miao, R. Ma, W. Zhao, L. Ren, G. Zhang, L. Zhai, D. Wang, S. Dou, Synthesis and magnetic properties of monodisperse $CoFe_2O_4$ nanoparticles coated by SiO_2, Ceram. Int. 44 (2018) 22462–22466, https://doi.org/10.1016/j.ceramint.2018.09.014.
[41] J.M.N. dos Santos, C.R. Pereira, L.A.A. Pinto, T. Frantz, É.C. Lima, E.L. Foletto, G.L. Dotto, Synthesis of a novel $CoFe_2O_4$/chitosan magnetic composite for fast adsorption of indigotine blue dye, Carbohydr. Polym. 217 (2019) 6–14, https://doi.org/10.1016/j.carbpol.2019.04.054.
[42] T. Li, F. Song, J. Zhang, S. Liu, B. Xing, Y. Bai, Pyrolysis characteristics of soil humic substances using TG-FTIR-MS combined with kinetic models, Sci. Total Environ. 698 (2020) 134237, , https://doi.org/10.1016/j.scitotenv.2019.134237.
[43] J. Liu, Z. Zhao, G. Jiang, Coating Fe_3O_4 magnetic nanoparticles with humic acid for high efficient removal of heavy metals in water, Environ. Sci. Technol. 42 (2008) 6949–6954, https://doi.org/10.1021/es800924c.
[44] R. Qu, C. Sun, M. Wang, C. Ji, Q. Xu, Y. Zhang, C. Wang, H. Chen, P. Yin, Adsorption of Au(III) from aqueous solution using cotton fiber/chitosan composite adsorbents, Hydrometallurgy. 100 (2009) 65–71, https://doi.org/10.1016/j.hydromet.2009.10.008.
[45] M. Grigorova, H.J. Blythe, V. Blaskov, V. Rusanov, V. Petkov, V. Masheva, D. Nihtianova, L.M. Martinez, J.S. Muñoz, M. Mikhov, Magnetic properties and Mössbauer spectra of nanosized CoFe2O4 powders, J. Magn. Magn. Mater. 183 (1998) 163–172, https://doi.org/10.1016/S0304-8853(97)01031-7.
[46] Y. Narita, S.C.W. Sakti, Y. Akemoto, S. Tanaka, Ultra-rapid removal of cationic organic dyes by novel single- and double-stranded DNA immobilized on quaternary ammonium magnetic chitosan, J. Environ. Chem. Eng. 7 (2019) 103308, , https://doi.org/10.1016/j.jece.2019.103308.
[47] R. Foroutan, R. Mohammadi, J. Razeghi, B. Ramavandi, Performance of algal activated carbon / Fe_3O_4 magnetic composite for cationic dyes removal from aqueous solutions, Algal Res. 40 (2019), https://doi.org/10.1016/j.algal.2019.101509.
[48] M. Gao, Z. Wang, C. Yang, J. Ning, Z. Zhou, G. Li, Novel magnetic graphene oxide decorated with persimmon tannins for efficient adsorption of malachite green from aqueous solutions, Colloids Surf. A Physicochem. Eng. Asp. 566 (2019) 48–57, https://doi.org/10.1016/j.colsurfa.2019.01.016.
[49] X. Li, H. Lu, Y. Zhang, F. He, L. Jing, X. He, Fabrication of magnetic alginate beads with uniform dispersion of $CoFe_2O_4$ by the polydopamine surface functionalization for organic pollutants removal, Appl. Surf. Sci. 389 (2016) 567–577, https://doi.org/10.1016/j.apsusc.2016.07.162.
[50] S. Lagergren, About the theory of so-called adsorption of soluble substance, K. Sven, K. Handlingar Tidskr. 24 (1898) 1–39.
[51] Y. Ho, The kinetics of sorption of divalent metal ions onto sphagnum moss peat, Water Res. 34 (2000) 735–742, https://doi.org/10.1016/S0043-1354(99)00232-8.
[52] S.Y. Elovich, O.G. Larionov, Theory of adsorption from solutions of non electrolytes on solid (I) equation adsorption from solutions and the analysis of its simplest form, (II) verification of the equation of adsorption isotherm from solutions, Izv. Akad. Nauk. SSSR, Otd. Khimicheskikh Nauk. 2 (1962) 209–216.
[53] H.M. Freundlich, Uber die adsorption in losungen, Zeitschrift Für Phys. Chemie. 57 (1906) 385–470.
[54] I. Langmuir, The adsorption of gases on plane surfaces of glass, mica and platinum, J. Am. Chem. Soc. 40 (1918) 1361–1403, https://doi.org/10.1021/ja02242a004.
[55] M. Temkin, V. Pyzhev, Recent modification to Langmuir isotherms, Acta Physchim. 12 (1950) 217.
[56] C.H. Giles, T.H. MacEwan, S.N. Nakhwa, D. Smith, 786. Studies in adsorption. Part XI. A system of classification of solution adsorption isotherms, and its use in diagnosis of adsorption mechanisms and in measurement of specific surface areas of solids, J. Chem. Soc. (1960) 3973–3993, https://doi.org/10.1039/JR9600003973.
[57] M. Foroughi-Dahr, H. Abolghasemi, M. Esmaieli, G. Nazari, B. Rasem, Experimental study on the adsorptive behavior of congo red in cationic surfactant-modified tea waste, Process Saf. Environ. Prot. 95 (2015) 226–236, https://doi.org/10.1016/j.psep.2015.03.005.
[58] E.C. Lima, A. Hosseini-Bandegharaei, J.C. Moreno-Piraján, I. Anastopoulos, A critical review of the estimation of the thermodynamic parameters on adsorption equilibria. Wrong use of equilibrium constant in the Van't Hoof equation for calculation of thermodynamic parameters of adsorption, J. Mol. Liq. 273 (2019) 425–434, https://doi.org/10.1016/j.molliq.2018.10.048.
[59] L. Ai, H. Huang, Z. Chen, X. Wei, J. Jiang, Activated carbon/$CoFe_2O_4$composites: Facile synthesis, magnetic performance and their potential application for the removal of malachite green from water, Chem. Eng. J. 156 (2010) 243–249, https://doi.org/10.1016/j.cej.2009.08.028.
[60] X. Liu, S. An, X. Zhou, L. Zhang, Y. Zhang, W. Shi, J. Yang, Comparative studies of removal of methyl green and basic fuchsin from wastewater by a novel magnetic nanoparticles Mg-Ferrites, J. Dispers. Sci. Technol. 35 (2014) 1727–1736, https://doi.org/10.1080/01932691.2013.871553.
[61] F. Keyhanian, S. Shariati, Magnetite nanoparticles with surface modification for removal of methyl violet from aqueous solutions, Arab J. Chem 9 (2016) 348–354, https://doi.org/10.1016/j.arabjc.2011.04.012.
[62] X. Hou, J. Feng, X. Liu, Y. Ren, Z. Fan, T. Wei, J. Meng, M. Zhang, Synthesis of 3D porous ferromagnetic $NiFe_2O_4$ and using as novel adsorbent to treat wastewater, J. Colloid Interface Sci. 362 (2011) 477–485, https://doi.org/10.1016/j.jcis.2011.06.070.
[63] F. Zhang, Z. Wei, W. Zhang, H. Cui, Effective adsorption of malachite green using magnetic barium phosphate composite from aqueous solution, Spectrochim. Acta - Part A Mol. Biomol. Spectrosc. 182 (2017) 116–122, https://doi.org/10.1016/j.saa.2017.03.066.

Re-collectable and recyclable epichlorohydrin-crosslinked humic acid with spinel cobalt ferrite core for simple magnetic removal of cationic triarylmethane dyes in polluted water

ORIGINALITY REPORT

15%	9%	13%	4%
SIMILARITY INDEX	INTERNET SOURCES	PUBLICATIONS	STUDENT PAPERS

PRIMARY SOURCES

1	Satya Candra Wibawa Sakti, Rizki Ainuna Wijaya, Nindayu Indrasari, Mochamad Zakki Fahmi et al. "Magnetic hollow buoyant alginate beads achieving rapid remediation of oil contamination on water", Journal of Environmental Chemical Engineering, 2021 Publication	3%
2	Yasuyuki Narita, Satya Candra Wibawa Sakti, Yasuhiro Akemoto, Shunitz Tanaka. "Ultra-rapid removal of cationic organic dyes by novel single- and double-stranded DNA immobilized on quaternary ammonium magnetic chitosan", Journal of Environmental Chemical Engineering, 2019 Publication	3%
3	explore.openaire.eu Internet Source	1%
4	Quanyuan Chen, Yuan Yao, Zheying Zhao, Juan Zhou, Zhao Chen. "Long term catalytic	<1%

activity of pyrite in Heterogeneous Fenton-like oxidation for the tertiary treatment of dyeing wastewater", Journal of Environmental Chemical Engineering, 2021
Publication

5	Satya Candra Wibawa Sakti, Yasuyuki Narita, Takahiro Sasaki, Nuryono, Shunitz Tanaka. "A novel pyridinium functionalized magnetic chitosan with pH-independent and rapid adsorption kinetics for magnetic separation of Cr(VI)", Journal of Environmental Chemical Engineering, 2015 Publication	<1 %
6	hrcak.srce.hr Internet Source	<1 %
7	pub.epsilon.slu.se Internet Source	<1 %
8	Fan Zhang, Zhong Wei, Wanning Zhang, Haiyan Cui. "Effective adsorption of malachite green using magnetic barium phosphate composite from aqueous solution", Spectrochimica Acta Part A: Molecular and Biomolecular Spectroscopy, 2017 Publication	<1 %
9	Submitted to University of Babylon Student Paper	<1 %
10	Submitted to University of KwaZulu-Natal Student Paper	

		<1 %
11	edoc.ub.uni-muenchen.de Internet Source	<1 %
12	eprints.soton.ac.uk Internet Source	<1 %
13	M.B.B. Pereira, L.M.C. Honório, C.G. Lima-Júnior, E.C. Silva Filho, Fabrice Gaslain, B. Rigaud, M.G. Fonseca, M. Jaber. "Modulating the structure of organofunctionalized hydroxyapatite/tripolyphosphate/chitosan spheres for dye removal", Journal of Environmental Chemical Engineering, 2020 Publication	<1 %
14	www.doria.fi Internet Source	<1 %
15	Zhu, Hua-Yue, Ru Jiang, Yong-Qian Fu, Rong-Rong Li, Jun Yao, and Sheng-Tao Jiang. "Novel multifunctional NiFe2O4/ZnO hybrids for dye removal by adsorption, photocatalysis and magnetic separation", Applied Surface Science, 2016. Publication	<1 %
16	El-Khamssa Guechi, Oualid Hamdaoui. " Biosorption of methylene blue from aqueous solution by potato ( ) peel: equilibrium modelling, kinetic, and thermodynamic	<1 %

studies ", Desalination and Water Treatment, 2015
Publication

17	Submitted to University of California, Merced Student Paper	<1 %
18	www.jstage.jst.go.jp Internet Source	<1 %
19	repositorio.ulima.edu.pe Internet Source	<1 %
20	www.i-scholar.in Internet Source	<1 %
21	www.infona.pl Internet Source	<1 %
22	www.oiirj.org Internet Source	<1 %
23	Submitted to Amity University Student Paper	<1 %
24	Satya Candra Wibawa Sakti, Dwi Siswanta, Nuryono. "Adsorption of gold(III) on ionic imprinted amino-silica hybrid prepared from rice hull ash", Pure and Applied Chemistry, 2012 Publication	<1 %
25	Seyedeh Sadrieh Emadian, Mohsen Ghorbani, Gholamreza Bakeri. "Magnetically separable CoFe2O4/ZrO2 nanocomposite for the	<1 %

photocatalytic reduction of hexavalent chromium under visible light irradiation", Synthetic Metals, 2020
Publication

26	asr.urmia.ac.ir Internet Source	<1 %
27	bmcchem.biomedcentral.com Internet Source	<1 %
28	ethesis.nitrkl.ac.in Internet Source	<1 %
29	Submitted to University of Nottingham Student Paper	<1 %
30	www.eurjchem.com Internet Source	<1 %
31	Submitted to Curtin University of Technology Student Paper	<1 %
32	Jiangdong Dai, Zhiping Zhou, Chunyan Zhao, Xiao Wei, Xiaohui Dai, Lin Gao, Zhijing Cao, Yongsheng Yan. "Versatile Method To Obtain Homogeneous Imprinted Polymer Thin Film at Surface of Superparamagnetic Nanoparticles for Tetracycline Binding", Industrial & Engineering Chemistry Research, 2014 Publication	<1 %
33	Zhang, Lei, Yunyu Zhang, Lijun Yang, Xiaoqing Jiang, and Qi Yang. "A rapid method for the	<1 %

removal of Methyl blue dye from wastewater by magnetic nanoparticles Mn-ferrites", Desalination and Water Treatment, 2015.
Publication

---

34 documents.mx
Internet Source
<1%

---

35 Fabrício Ravanello Mariosi, Janio Venturini, Alexandre da Cas Viegas, Carlos Perez Bergmann. "Lanthanum-doped spinel cobalt ferrite (CoFe2O4) nanoparticles for environmental applications", Ceramics International, 2020
Publication
<1%

---

36 Juliana M.N. dos Santos, Carolina R. Pereira, Luiz Antonio A. Pinto, Tuanny Frantz et al. "Synthesis of a novel CoFe2O4/chitosan magnetic composite for fast adsorption of indigotine blue dye", Carbohydrate Polymers, 2019
Publication
<1%

---

37 Rauf Foroutan, Reza Mohammadi, Jafar Razeghi, Bahman Ramavandi. "Performance of algal activated carbon/Fe3O4 magnetic composite for cationic dyes removal from aqueous solutions", Algal Research, 2019
Publication
<1%

---

38 de Melo, Bruna Alice Gomes, Fernanda Lopes Motta, and Maria Helena Andrade Santana.
<1%

"Humic acids: Structural properties and multiple functionalities for novel technological developments", Materials Science and Engineering C, 2016.
Publication

39	digital.csic.es Internet Source	<1 %
40	eprints.kfupm.edu.sa Internet Source	<1 %
41	www.arkat-usa.org Internet Source	<1 %
42	Ghaedi, M.. "Kinetics, thermodynamics and equilibrium evaluation of direct yellow 12 removal by adsorption onto silver nanoparticles loaded activated carbon", Chemical Engineering Journal, 20120401 Publication	<1 %
43	aip.scitation.org Internet Source	<1 %
44	cest2018.elmergib.edu.ly Internet Source	<1 %
45	hal.sorbonne-universite.fr Internet Source	<1 %
46	repositorio.unesp.br Internet Source	<1 %

sioc-journal.cn

47	Internet Source	<1%
48	trepo.tuni.fi Internet Source	<1%
49	www.gums.ac.ir Internet Source	<1%
50	www.intechopen.com Internet Source	<1%
51	www.scielo.br Internet Source	<1%
52	A.I. Ivanets, V. Srivastava, M.Yu. Roshchina, M. Sillanpää, V.G. Prozorovich, V.V. Pankov. "Magnesium ferrite nanoparticles as a magnetic sorbent for the removal of Mn 2+ , Co 2+ , Ni 2+ and Cu 2+ from aqueous solution", Ceramics International, 2018 Publication	<1%
53	Ai, L.. "Removal of methylene blue from aqueous solution by a solvothermal-synthesized graphene/magnetite composite", Journal of Hazardous Materials, 20110915 Publication	<1%
54	Anirudhan, T.S.. "Chromium(III) removal from water and wastewater using a carboxylate-functionalized cation exchanger prepared	<1%

from a lignocellulosic residue", Journal of Colloid And Interface Science, 20071215
Publication

55 Mehdi Rahimdokht, Elmira Pajootan, Mokhtar Arami. "Application of melon seed shell as a natural low-cost adsorbent for the removal of Methylene Blue from dye-bearing wastewaters: optimization, isotherm, kinetic, and thermodynamic", Desalination and Water Treatment, 2015 <1%
Publication

56 Shamik Chowdhury, Papita Das (Saha). "Mechanistic, Kinetic, and Thermodynamic Evaluation of Adsorption of Hazardous Malachite Green onto Conch Shell Powder", Separation Science and Technology, 2011 <1%
Publication

57 Si Chen, Chaoxian Qin, Teng Wang, Fangyuan Chen, Xuli Li, Haobo Hou, Min Zhou. "Study on the adsorption of dyestuffs with different properties by sludge-rice husk biochar: Adsorption capacity, isotherm, kinetic, thermodynamics and mechanism", Journal of Molecular Liquids, 2019 <1%
Publication

58 ascelibrary.org <1%
Internet Source

bjbas.springeropen.com

59	Internet Source	<1%
60	downloads.hindawi.com Internet Source	<1%
61	iwaponline.com Internet Source	<1%
62	lume.ufrgs.br Internet Source	<1%
63	neptjournal.com Internet Source	<1%
64	pesquisa.bvsalud.org Internet Source	<1%
65	rd.springer.com Internet Source	<1%
66	www.iaeme.com Internet Source	<1%
67	www.mrforum.com Internet Source	<1%
68	www.researchgate.net Internet Source	<1%
69	www.springerprofessional.de Internet Source	<1%
70	Chunyan Zhao, Jiangdong Dai, Zhiping Zhou, Xiaohui Dai, Yongli Zou, Ping Yu, Tianbian Zou,	<1%

Chunxiang Li, Yongsheng Yan. "One-pot method for obtaining hydrophilic tetracycline-imprinted particles via precipitation polymerization in ethanol", Journal of Applied Polymer Science, 2014
Publication

---

71 Yongli Zou, Chunyan Zhao, Jiangdong Dai, Zhiping Zhou, Jianming Pan, Ping Yu, Yongsheng Yan, Chunxiang Li. "Magnetic and hydrophilic imprinted particles via ATRP at room temperature for selective separation of sulfamethazine", Colloid and Polymer Science, 2013 <1%
Publication

Exclude quotes	On	Exclude matches	< 5 words
Exclude bibliography	On		

Re-collectable and recyclable epichlorohydrin-crosslinked humic acid with spinel cobalt ferrite core for simple magnetic removal of cationic triarylmethane dyes in polluted water

GRADEMARK REPORT

FINAL GRADE

/0

GENERAL COMMENTS

Instructor

PAGE 1

PAGE 2

PAGE 3

PAGE 4

PAGE 5

PAGE 6

PAGE 7

PAGE 8

PAGE 9

PAGE 10

PAGE 11

PAGE 12

PAGE 13

PAGE 14